FORSCHUNGSZENTRUM KARLSRUHE

Technik und Umwelt

Wissenschaftliche Berichte

FZKA 6362

THE STELLAR (n, γ) CROSS SECTION OF ^{180m}Ta, THE RAREST STABLE ISOTOPE IN NATURE

K. WISSHAK, F. VOSS, C. ARLANDINI, F. KÄPPELER, M. HEIL, R. REIFARTH, M. KRTIČKA[1], and F. BEČVÁŘ[1]

Institut für Kernphysik

[1]Charles University, Prague, Czech Republic

Forschungszentrum Karlsruhe GmbH, Karlsruhe
2000

ABSTRACT

The neutron capture cross section of ^{180m}Ta has been measured between 10 and 100 keV in a time-of-flight experiment at the Karlsruhe 3.7 MV Van de Graaff accelerator. Neutrons were produced via the ^{7}Li$(p,n)^{7}$Be reaction by bombarding metallic Li targets with a pulsed proton beam, and gold was used as a cross section standard. Though the world supply of enriched ^{180m}Ta was available for this experiment, the sample consisted of 150 mg Ta_2O_5 enriched to only 5.5% in ^{180m}Ta. The difficult separation of the comparably few capture events in ^{180m}Ta from the much larger background due to captures in ^{181}Ta could be achieved by means of the Karlsruhe 4π Barium Fluoride Detector, taking advantage of its combination of high efficiency, good energy resolution, and high granularity. The cross section was determined with an overall uncertainty of better than 10% in the energy range from 30 to 100 keV and could be used for renormalizing statistical model calculations outside the investigated energy range, which had predicted about two times larger values. Based on these data, Maxwellian averaged neutron capture cross sections were calculated for thermal energies between $kT = 8$ and 100 keV. Together with the result of a recent photoactivation experiment, these data were used for a detailed s-process analysis, which indicates that ^{180m}Ta is predominantly of s-process origin.

ZUSAMMENFASSUNG

DER STELLARE (n,γ) QUERSCHNITT VON ^{180m}Ta, DEM SELTENSTEN STABILEN ISOTOP IN DER NATUR

Der Neutroneneinfangquerschnitt von ^{180m}Ta wurde von 10 bis 100 keV in einem Flugzeitexperiment am Karlsruher Van de Graaff Beschleuniger relativ zum (n,γ)–Querschnitt von Gold als Standard gemessen. Neutronen wurden über die ^{7}Li(p,n)^{7}Be–Reaktion durch Beschuß metallischer Li–Targets mit einem gepulsten Protonenstrahl erzeugt. Obwohl der Weltvorrat an angereichertem ^{180m}Ta zur Verfügung stand, bestand die Probe lediglich aus 150 mg Ta_2O_5 mit einem ^{180m}Ta Anteil von nur 5.5%. Die schwierige Trennung der vergleichsweise seltenen Einfangereignisse am ^{180m}Ta von dem erheblich grösseren Untergrund durch Einfänge am ^{181}Ta konnte mit dem Karlsruher 4π Barium Fluorid Detektors dank dessen Kombination von hoher Ansprechwahrscheinlichkeit, guter Energieauflösung und hoher Granularität realisiert werden. Der Wirkungsquerschnitt wurde im Energiebereich von 30 bis 100 keV mit einer Genauigkeit von besser als 10% bestimmt. Damit konnten mit dem statistischen Modell vorhergesagte Werte ausserhalb des untersuchten Energiebereichs, die einen Faktor zwei höher lagen, renormiert werden. Auf dieser Grundlage wurden die stellaren Einfangquerschnitte für thermische Energien von $kT = 8$ bis 100 keV berechnet. Zusammen mit dem Ergebnis einer neuen Photoaktivierung wurden mit diesen Daten eine detaillierte s-Prozess–Analyse durchgeführt, die nahelegt, dass ^{180m}Ta überwiegend im s-Prozess gebildet wurde.

Contents

1 INTRODUCTION

For two reasons ^{180m}Ta is a unique nucleus: It is the rarest stable isotope found in the solar system, representing only 0.012% of natural tantalum, which in turn is the rarest chemical element [1] in nature. Furthermore, it is the only isotope that is stable in the isomeric state, the ground state having a half life of 8.1 h.

The rarity of ^{180m}Ta reflects the difficulty of its production. In fact, at first glance the common processes for synthesizing the heavy elements, including the s, r, and p processes, seem to fail in case of ^{180m}Ta. Apart from the difficulty in producing it, ^{180m}Ta may be even easily destroyed in the hot stellar interior by thermally induced depopulation to the short–lived ground state.

Obviously, ^{180m}Ta ows its existence to a fine balance of nuclear and stellar parameters. Therefore it is long recognized to represent an important test for nucleosynthesis models of the heavy elements and attracted continuous efforts in experimental nuclear physics as well as in theoretical astrophysics. For the crucial nuclear part experiments were severely hampered by the lack of samples and/or sufficiently sensitive techniques, often allowing only qualitative statements to be made. This challenge motivated a whole series of recent approaches aiming at more quantitative solutions.

The s process is certainly most suited for a quantitative description of the corresponding ^{180m}Ta yield, since the reaction path follows the valley of β stability and is, therefore, directly accessible to laboratory studies. Also from the astrophysical side the associated He burning scenarios are comparably stable and easier to model than the explosive scenarios responsible for the r and p processes.

The s-process path in the region of ^{180m}Ta is sketched in Fig. 1 and shows that the main reaction flow (thick arrows) is bypassing ^{180m}Ta completely, since ^{181}Hf appears to be the first unstable hafnium isotope. Nevertheless, marginal feeding of ^{180m}Ta can be achieved in two weak branchings of the main reaction path. The decay of the 8^- isomeric state in ^{180}Hf, which is weekly populated in neutron capture of ^{179}Hf has been suggested by Beer and Ward [2] and has been shown by Kellog and Norman [3] to account for about 20% of the ^{180m}Ta abundance. Population of this ^{180}Hf isomer at the termination of the β-decay chain at A=180 was found negligibly small, thus excluding a possible additional r-process contribution [4].

While the s contribution via the ^{180}Hf decay is fixed by the partial cross section feeding the 8^- isomer, the second branching suggested by Yokoi and Takahashi [5] is mostly determined by the stellar conditions of the s-process site. These authors pointed out that the $7/2^-$ state at 214 keV in ^{179}Hf, which is thermally populated in the hot stellar photon bath, is unstable against β-decay to ^{179}Ta. In spite of the back decay, this leads to a small ^{179}Ta abundance which acts as a seed for neutron captures to ^{180m}Ta. In contrast to the first branching, this route depends strongly on temperature, indicating that the ^{180m}Ta abundance may be interpreted as a sensitive stellar thermometer [6].

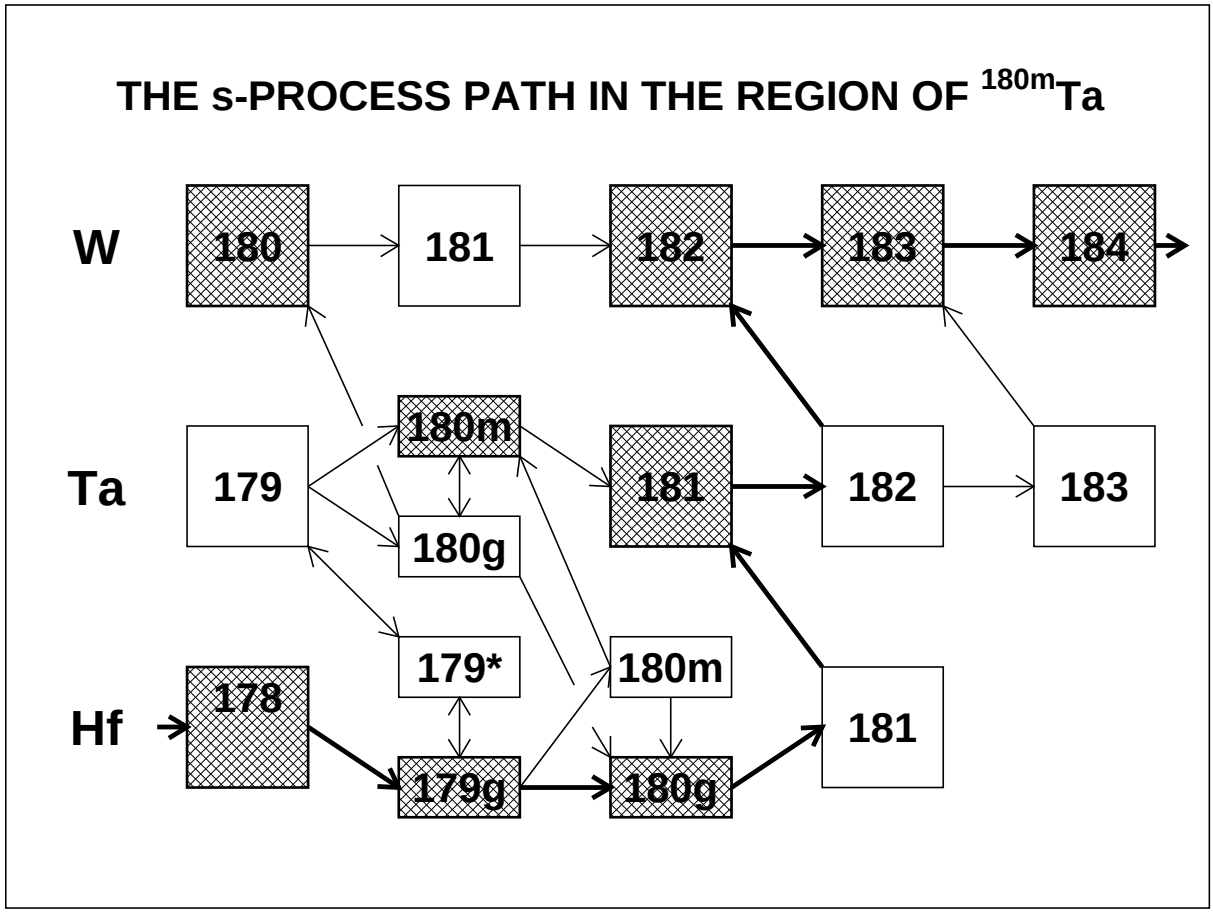

Figure 1: The reaction path of the s process in the Hf/Ta/W region. Though the main reaction path (thick arrows) is bypassing ^{180m}Ta this rare isotope is produced via weak branchings due to neutron captures on ^{179}Ta and β-decays of a weakly populated isomer in ^{180}Hf.

Since the second branching opens only at relatively high temperatures its efficiency for producing ^{180m}Ta is intimately linked with the possibility that the freshly produced ^{180m}Ta may be immediately destroyed by thermally induced depopulation to the short-lived ground state [6]. Direct decays being forbidden by selection rules, this depopulation can only be achieved by excitation of an intermediate state with decay channels to the ground state. Many attempts have been made to locate the position of the lowest intermediate state because this determines the fate of ^{180m}Ta: Only if this state appears above or near 1 MeV excitation energy, ^{180m}Ta may well survive at typical s-process temperatures.

A variety of photoactivation experiments have been performed by exposing natural Ta to photon fields of bremsstrahlung facilities [7, 8, 9, 10] and strong γ-ray sources [6, 11, 12] or by using Coulomb excitation [13, 14]. All these efforts were hampered by the use of natural samples. Therefore, the experimental sensitivity was not sufficient to identify any mediating states below an excitation energy of 1.5 MeV.

Experimental data were also missing for the neutron capture rates which determine

the destruction and production of ^{180m}Ta. The available calculated ^{180m}Ta cross sections differed by almost a factor two [6, 15, 16], and for neutron capture on ^{179}Ta the presently adopted value [6] is even three times smaller than calculated by Holmes et al. [16].

In an attempt to improve the nuclear physics part of the this pending situation a Munich - Stuttgart - Darmstadt - Karlsruhe collaboration shared the loan of the world supply of enriched ^{180m}Ta . This sample consisted of 150 mg tantalum oxide powder with a ^{180m}Ta enrichment of only 5.5%. Nevertheless, it allowed to improve the sensitivity of previous photoactivation experiments by a factor of 5000, resulting in the discovery of several new mediating states [17]. The same sample could then be used for the measurement of the neutron capture cross section in the energy range from 10 to 100 keV reported here.

The results of both experiments bear important consequences for the origin of ^{180m}Ta and for testing current s process models. Since the schematic classical approach [18] turned out to fail in describing the s abundances near magic neutron numbers and in certain branchings [19] it became obvious that this heuristic model is particularly unfit to account for the weak and delicate branchings to ^{180m}Ta: While the production via the ^{180m}Hf isomer is not affected by the stellar environment, the second branching depends strongly on temperature because the population of the β-unstable excited states in ^{179}Hf is determined by thermally induced transitions. The improved photoactivation experiment [17] showed that the half-life of ^{180m}Ta is reduced to less than 10 yr for temperatures in excess of T_8=2 (T_8 = temperature in units of 10^8 K). In view of the physical conditions characteristic for the classical approach, i.e. temperatures of T_8=2.5$\pm$0.4 and a duration of 10^4 y [20], this implies that ^{180m}Ta could not survive in the s process.

For the more complex stellar s-process model, however, the fate of ^{180m}Ta is completely different. It is currently accepted that the main s-process component between A=100 and 200 is produced during recurrent thermal instabilities in the AGB phase of 1.5 to 3 $M_\odot$ mass stars [21, 22, 23]. In this scenario, about 95% of the neutron irradiation occurs via the ^{13}C(α, n) reaction between thermal instabilities at comparably low temperatures of T_8=1, where ^{179}Hf and ^{180m}Ta are both stable. Accordingly, only a minor fraction of ^{180m}Ta is produced via the decay of ^{180m}Hf. During thermal instabilities, however, temperatures of T_8=2.5 - 2.8 are reached for a few years, resulting in a second neutron burst due to the activation of the ^{22}Ne(α, n) reaction. At these higher temperatures, ^{179}Hf becomes unstable, thus opening the neutron capture sequence from ^{179}Ta to ^{180m}Ta. Since the prolific energy production in these He shell flashes creates a highly convective zone with turnover times of less than a week [24], freshly produced ^{180m}Ta is effectively mixed into cooler regions where it survives and from where it is eventually mixed into the stellar envelope.

Calculations using theoretically calculated Ta cross sections and neglecting a possible thermal destruction of ^{180m}Ta find that about 50% of the solar ^{180m}Ta abundance can be accounted for by this stellar model [19]. Obviously, any attempt for a more realistic and quantitative description of the s-process origin of this isotope has to consider the important thermal effect on the life time of ^{180m}Ta and must be based on a reliable experimental value for the stellar (n,γ) cross section. This improved nuclear physics input is mandatory for solving this long standing astrophysical puzzle and for interpreting the ^{180m}Ta abundance as a constraint for the temperature profile and the convective time

scale during He shell flashes on the AGB.

Apart from the negligible r-process yields mentioned before, the p and/or ν processes may have contributed to the production of ^{180m}Ta as well. Since both processes are related to supernovae, thermal depopulation is of minor importance in these cases due the short time scale of the explosion.

The p process is related to the explosive Ne-O burning where temperatures of T_9=2-3 are reached. The high energy part of the thermal photon distribution gives rise to successive (γ, n) reactions, driving the reaction path to the proton rich side by about 5 mass units until the rapidly increasing neutron separation energies favor the competing (γ, p) and (γ,α) channels. Hence, the p process reaction network remains relatively close to stability. At freeze-out, the primary reaction products decay by β^+ and EC transitions and account for the rare proton rich species.

Though the p process contributes an almost negligible fraction of the heavy element abundances and though ^{180m}Ta is shielded from the main p-process yields by its stable isobar ^{180}W, a small but significant ^{180m}Ta abundance may result from direct (γ, n) reactions on the abundant ^{181}Ta. Studies of this scenario led to somewhat contradictory results. While Prantzos et al. claimed a significant production for the p process in supernova 1987a [25], Rayet *et al.* [26] found in a systematic study of typical p-process scenarios that ^{180m}Ta is depleted under the conditions of explosive Ne/O burning. On the other hand, a more recent study of the p process in type II supernovae yields again a significant overproduction of ^{180m}Ta [27].

The ν process suggested by Woosley *et al.* [28] considers that inelastic neutrino scattering and subsequent neutron evaporation may affect the abundance pattern when the intense neutrino flux of a supernova explosion interacts with the outer layers. It was found that this mechanism contributes especially to the rare ^{180m}Ta which could be efficiently produced in this way.

These supernova scenarios for the production of ^{180m}Ta need to be investigated by more quantitative analyses with particular emphasis on the nuclear reaction aspects, e.g. by considering the relative population of short-lived ground state and quasi-stable isomer.

The present (n, γ) measurements are described in Sec. 2, followed by the data analysis (Sec. 3) and a discussion of the results and uncertainties (Secs. 4 and 5). The stellar cross sections are presented in Sec. 6, and the astrophysical consequences outlined in Sec. 7.

2 EXPERIMENT

The neutron capture cross section of ^{180m}Ta was measured in the energy range from 10 to 100 keV using gold as a standard. Since the experimental method has been published in detail [29, 30, 31, 32], only a general description is given here, complemented with the specific features of the present measurement

Neutrons were produced via the ^{7}Li$(p, n)^7$Be reaction by bombarding metallic Li targets with the pulsed proton beam of the Karlsruhe 3.7 MV Van de Graaff accelerator. The neutron energy was determined by time of flight (TOF), the samples being located

at a flight path of 79 cm. The relevant parameters of the accelerator were a pulse width of <1 ns, a repetition rate of 250 kHz, and an average beam current of 1.8 μA. In two different runs, the proton energies were adjusted 20 and 30 keV above the threshold of the ^{7}Li$(p,n)^{7}$Be reaction at 1.881 MeV, resulting in continuous neutron spectra in the energy range from 10 to 80 keV and 5 to 100 keV, respectively. The first spectrum was considered because it yielded a significantly better signal-to-background ratio around 30 keV. The background was further reduced by means of a collimator which provided a well defined neutron beam of 15 mm diameter at the sample position.

Capture events were registered with the Karlsruhe 4π BaF_2 detector via the prompt capture γ–ray cascades. This detector consists of 41 hexagonal and pentagonal crystals forming a spherical shell of BaF_2 with 10 cm inner radius and 15 cm thickness. It is characterized by a resolution in γ–ray energy of 7% at 2.5 MeV, a time resolution of 500 ps, and a peak efficiency of 90% at 1 MeV. The 1.7 MeV threshold in γ–ray energy used in the present experiment corresponds to an efficiency for capture events of more than 95%. (For a comprehensive description of this detector see Ref. [31]).

The experiment was divided into two runs using the conventional data acquisition technique with the detector operated as a calorimeter.

The present work was carried out with the same ^{180m}Ta sample that was used in the photoactivation experiment mentioned above [17]. Though it represented the world supply of isotopically enriched Ta_2O_5, it consisted of only 150 mg with a ^{180m}Ta content of 5.5%. This total amount of 6.7 mg ^{180m}Ta was significantly less than the 500 mg that are typically required for this type of cross section measurements. The sample of 11.5 mm diameter and 0.7 mm thickness was encapsulated in a flat graphite container. Identical containers were also used for a set of additional samples which was mounted on a sample ladder. It included a gold disk for determining the neutron flux, 150 mg natural tantalum oxyde for obtaining the isotopic correction, as well as an empty container for simulating the background due to scattered neutrons and measuring the background related to the container itself. Furthermore, an empty position on the sample ladder allowed to determine the sample-independent background. The relevant data characterizing these samples are compiled in Table 1.

As a consequence of the value of the enriched material and due to the requirements of the related photoactivation study the sample container could not be optimized for the present experiment. Accordingly, there were 100 times more carbon than tantalum atoms in the neutron beam. With respect to the ^{180m}Ta content this factor is again 20 times larger, which means that 6000 neutrons were scattered by the graphite container for each true capture event in ^{180m}Ta. The enormous background due to capture of these scattered neutrons in the BaF_2 crystals could only be discriminated by the unique combination of high efficiency, good energy resolution, and short flight path of the present setup. In a dedicated experiment, the container would have been made, for example, of 0.1 mm thick titanium, thus relaxing this problem by a factor 30 and allowing for a correspondingly better signal to background ratio.

In view of this difficulty, a first run with a maximum neutron energy of 100 keV was repeated with the maximum energy lowered to 80 keV. In this way, the integral neutron flux was reduced without changing the flux around 30 keV, resulting in a significantly better signal to background ratio in the important energy range from 20 to 50 keV.

The samples were put cyclically into the measuring position by a computer controlled device. The measuring time per sample of typically 10 min was defined by a beam current integrator. By averaging over 400 to 600 cycles per run (Table 2) long-term variations of the neutron yield were compensated. For each event, a 64 bit word was recorded on DAT tape containing sum energy, TOF information, and identification of the contributing detector modules. The experiment was restricted to this so-called calorimeter mode, because the small sample mass did not allow to achieve the counting statistics required for the ADC mode where the signals of all detector modules are recorded individually.

The parameters of the two runs with different maximum neutron energies are listed in Table 2.

Table 1: SAMPLE CHARACTERISTICS

Sample	Diameter	Thickness		Weight[a]	Container[b]	Neutron binding
	(mm)	(mm)	(10^{-3}at/barn)[c]	(g)	(g)	energy (MeV)
Empty						
^{197}Au	11.5	0.125	0.7427	0.2523	1.8343	6.513
^{180m}Ta[d]	11.5	0.7	0.3939	0.1501	1.8708	7.538
^{181}Ta	11.5	0.7	0.3933	0.1499	1.7680	6.063
Dummy					1.8702	

[a]For tantalum samples: weight of Ta_2O_5
[b]Graphite container, diameter 22 mm, thickness 3 mm
[c]For tantalum samples: sum of both Ta isotopes
[d]Isotopic composition: ^{180m}Ta 5.47±0.05%, ^{181}Ta 94.53±0.05%.

Table 2: PARAMETERS OF THE INDIVIDUAL RUNS

Run	Flight Path	TOF Scale	Number of Cycles	Maximum Neutron Energy	Measuring Time	Mode of Operation	Average Beam Current	Threshold in Sum Energy
	(mm)	(ns/ch)		(keV)	(d)		(μA)	(MeV)
I	788.4	0.7603	478	100	17.3	Calorimeter	2.0	1.7
II	788.5	0.7601	634	80	27.2	Calorimeter	1.6	1.7

3 DATA ANALYSIS

Most of the analysis of the neutron capture cross section was carried out in the same way as described previously [29, 30, 32].

3.1 Background subtraction

All events were sorted into two–dimensional spectra containing 128 sum energy versus 2048 TOF channels according to various event multiplicities (evaluation 1). In evaluation 2, this procedure was repeated by rejecting those events, where only neighboring detector modules contributed to the sum energy signal. With this option, background from the natural radioactivity of the BaF_2 crystals and from scattered neutrons can be reduced.

For all samples, the resulting spectra were normalized to equal neutron flux using the count rate of a ^{6}Li glass monitor close to the neutron target. The corresponding normalization factors are below 0.5% for all runs.

To some extent the rather poor signal to background ratio of the present experiment was compensated by the favorably large neutron separation energy and the high level density of the compound nucleus ^{181}Ta. This combination results in an average cascade multiplicity of 6.2, by far the largest value ever measured with the Karlsruhe 4π BaF_2 detector. Consequently, almost all capture events on ^{180m}Ta are observed with multiplicities $\geq$5. Therefore, the ^{180m}Ta cross section was evaluated only from these events which are much less affected by backgrounds than events with lower multiplicities. The missing fraction of low multiplicity events was determined by means of a computer simulation as described below. Furthermore, capture in the dominant ^{181}Ta impurity could be discriminated because of the smaller neutron separation energy of 6.1 MeV, resulting in a sum energy peak well below that of ^{180m}Ta at 7.6 MeV.

In the next step of data analysis, sample–independent backgrounds were removed by subtracting the spectrum measured with the empty position in the sample ladder. A remaining constant background was determined at very long flight times where no time–correlated events are expected. For run II, the corresponding two–dimensional spectra before and after these corrections are shown in Fig. 2 for the ^{181}Ta and ^{197}Au samples (event multiplicities >2).

The upper spectra are dominated by the constant background at low γ-ray energies and by the prompt γ-ray peak from the impact of the proton beam on the target. After subtraction of these sample-independent components the remaining background at high sum energies is due to capture of scattered neutrons in the BaF_2 crystals. The respective spectra for the ^{180m}Ta sample in Fig. 3 are restricted to events with multiplicities $\geq$5 and are given as a 32x32 channel matrix to average over the larger statistical fluctuations.

At this point, the spectra contain only events correlated with the sample. The next correction for isotopic impurities (see Ref.[29] for details) was performed by subtracting the properly normalized spectrum of the natural tantalum sample from the spectrum measured with the enriched sample. This step removes also most of the background from scattered neutrons, which is still dominant at this stage (see Fig. 3). The corresponding correction for the natural tantalum sample was negligible.

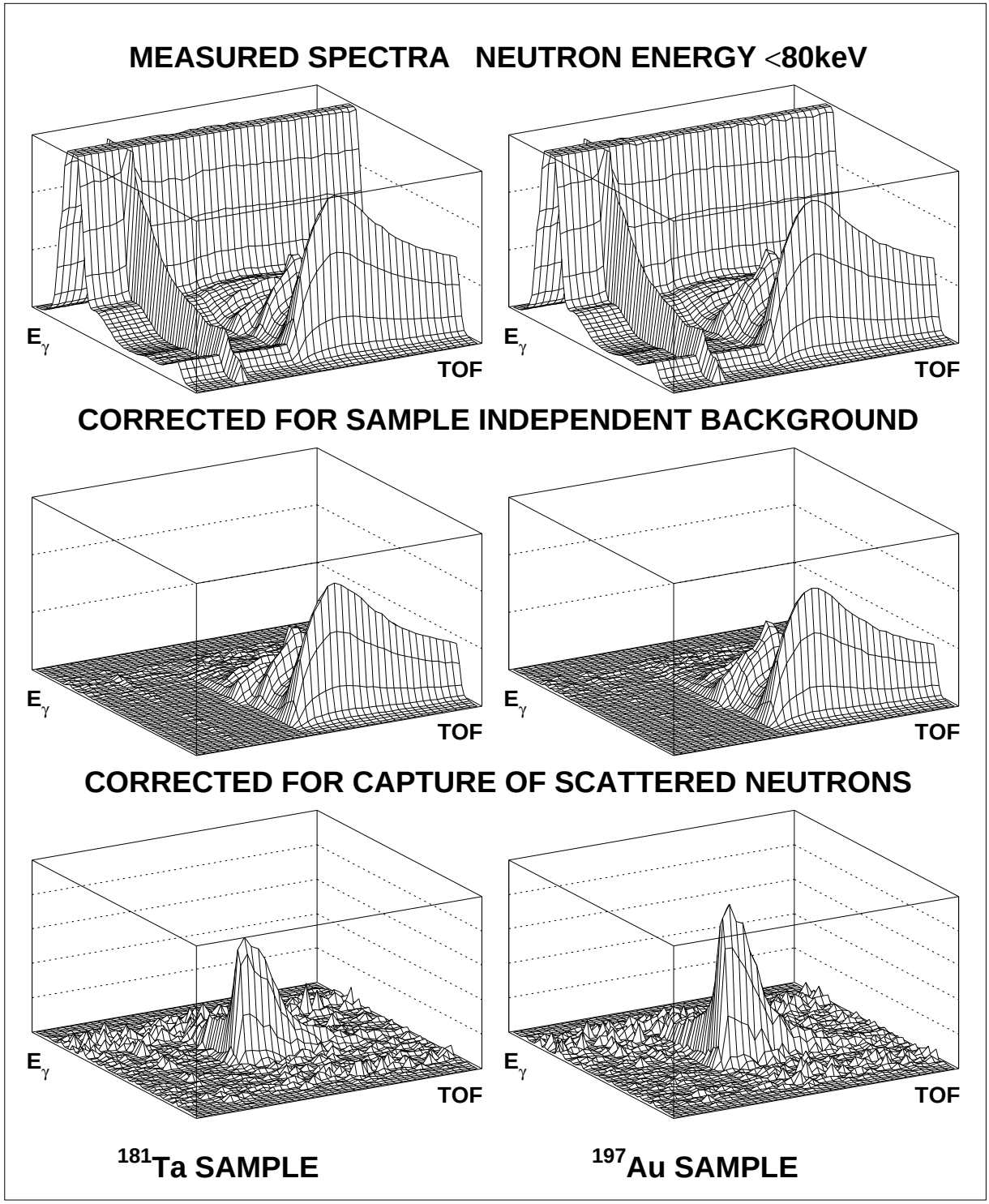

Figure 2: The different steps of background subtraction in the two–dimensional sum energy × TOF spectra. The data for ^{181}Ta and ^{197}Au were measured in run II with 80 keV maximum neutron energy and include events with multiplicity >2. The original spectrum of 128 × 2048 channels was compressed into a 64 × 64 channel matrix for better readability. In the bottom spectra the z-axes are stretched by a factor 6.

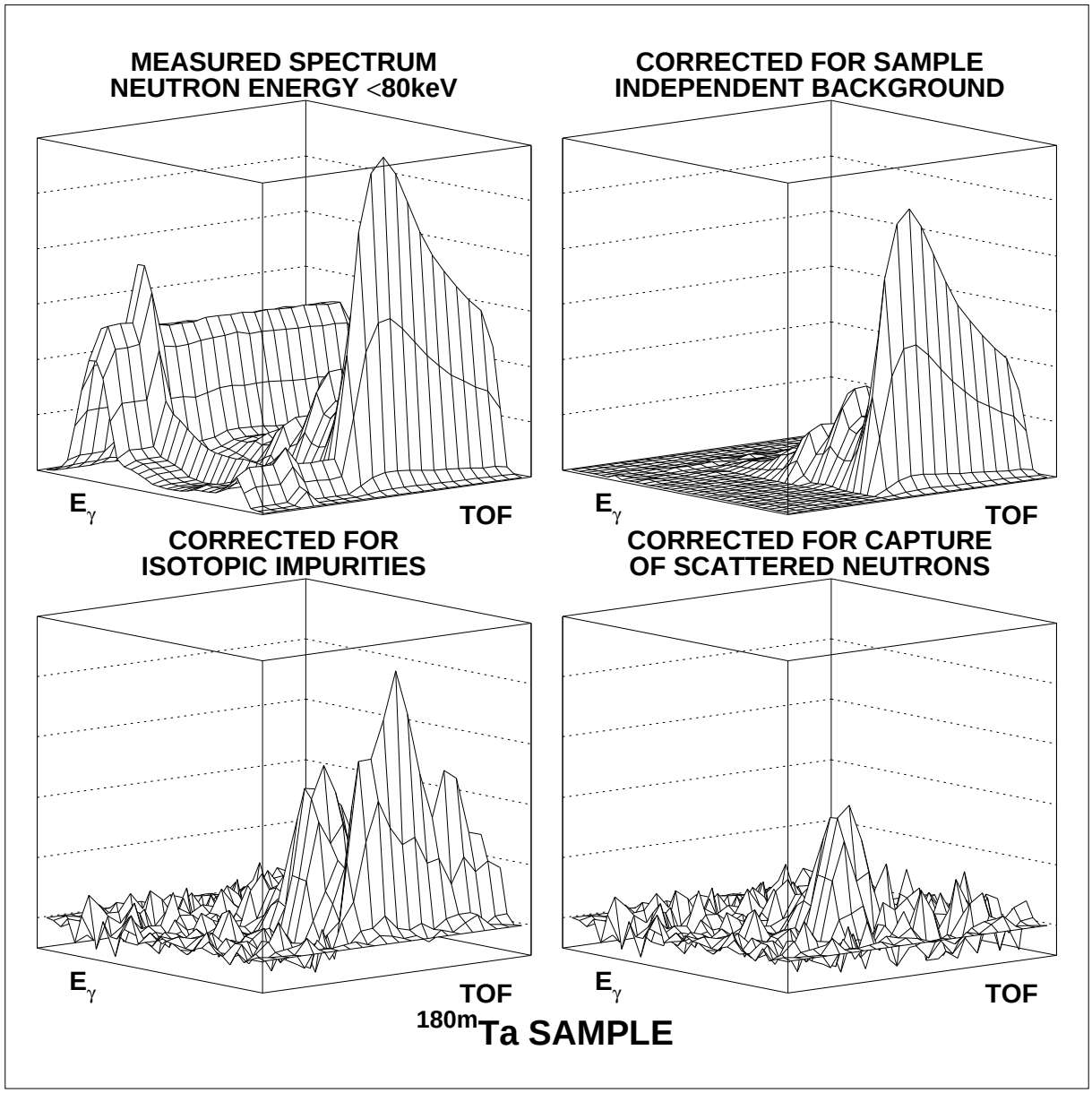

Figure 3: Same as Fig. 2 but for the ^{180m}Ta sample. The spectra contain only events with multiplicity $\geq$5. The original spectrum was compressed into a 32 $\times$ 32 channel matrix. The z-axes in the bottom spectra are stretched by a factor 24.

Fig. 4 shows the projection of the ^{180m}Ta spectrum onto the sum-energy axis before and after subtraction of the background from isotopic impurities. The upper spectrum is clearly dominated by background peaks from captures on the abundant ^{181}Ta impurity and from captures of scattered neutrons on the odd and even barium isotopes of the scintillator. The peak due to capture on ^{180m}Ta becomes evident in the corrected spectrum in the middle of Fig. 4, but exhibits a significant broadening compared to the background peaks.

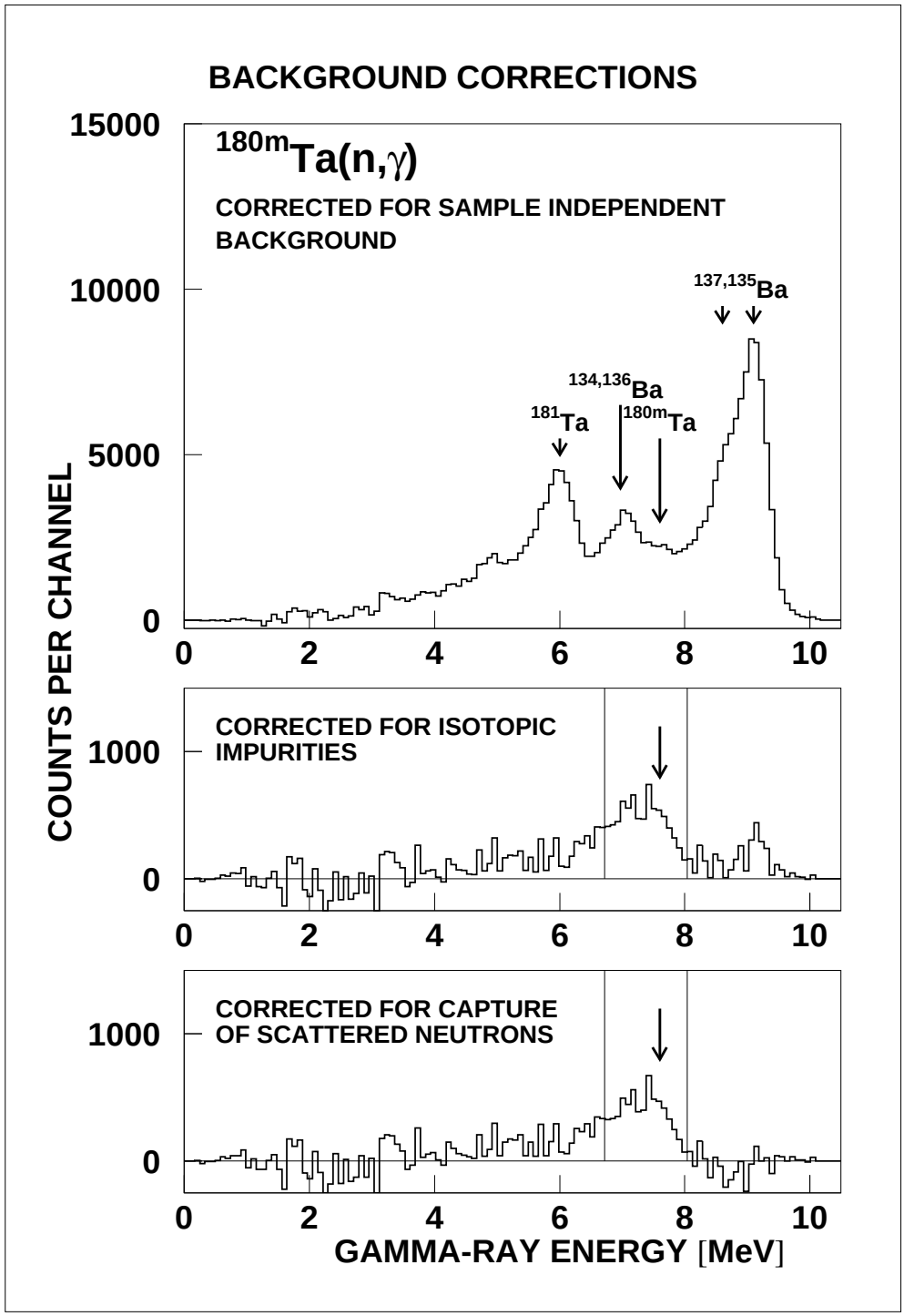

Figure 4: Sum energy spectra of the ^{180m}Ta sample before and after the corrections for isotopic impurities and capture of scattered neutrons. The energy range between 6.8 and 8 MeV that was used to determine the cross section as a function of neutron energy is indicated by vertical lines (see Fig. 5).

This broadening may be due to the population of isomeric states and/or due to a significant fraction of converted transitions. The population of isomeric states was observed

in neutron capture on several ytterbium isotopes [33]. If capture γ-ray cascades populate a level with a half-life longer than the experimental coincidence interval of about 30 ns, the following transitions to the ground state are not included in the sum energy signal. So far, only one state at 482 keV is known in ^{181}Ta with a half life of 10 ns, too short to cause the observed effect.

The occurrence of converted transitions was recently found responsible for the broadening of the sum energy peak in the spectrum of the gold standard (see below). Large multiplicities of the capture cascades imply a certain fraction of soft γ-transitions with sizable conversion coefficients in such high Z materials as gold and tantalum. These conversion electrons are easily absorbed before reaching the scintillator. Hence, their energy is missing in the recorded signals, resulting in a broadening of the sum energy peak.

It is to be emphasized that both effects correspond to a reduction of the effective cascade energy. Therefore, they are responsible for unrecognized systematic uncertainties in experiments using the pulse height weighting method, where the cascade energy is assumed to equal the sum of neutron separation energy and kinetic energy of the captured neutron. In contrast, experiments with the $4\pi BaF_2$ detector are not affected by these problems, since the detection efficiency is completely independent of the corresponding (minor) loss in resolution.

The evaluation of the ^{180m}Ta cross section as a function of neutron energy is based only on events with sum energies near the full energy peak as indicated in Fig. 4 by vertical lines. This region lying well above the capture events in ^{181}Ta ensures that background events due to capture of scattered neutrons are properly corrected by subtraction of the normalized spectrum of the ^{181}Ta sample. The respective TOF spectra shown in Fig. 5 were rebinned in order to improve the counting statistics per channel.

Following the correction for isotopic impurities, the remaining background due to capture of sample scattered neutrons was removed by means of the data measured with the scattering sample. Due to the comparably massive graphite container and the small sample mass this correction is unusually large. Fortunately, the binding energy of all investigated isotopes is below 7.6 MeV, thus allowing to use the strong peak due to capture in the odd barium isotopes between 8 and 10 MeV for normalization (see Fig. 4). Since this normalization is determined as a function of neutron TOF, the correction for scattered neutrons can be accurately treated in the entire energy range of this experiment. After this last step, the spectra contain only true capture events on the investigated isotopes (bottom spectra in Fig. 2 and last spectrum in Fig. 3). The corrections for capture of scattered neutrons are shown in the lower part of Fig. 5 and in Fig. 6.

The final TOF spectra in Figs. 7 and 8 were used to determine the cross section shape. Since the cross sections of ^{181}Ta and ^{197}Au exhibit to good approximation a $1/v$ dependence, the spectra of both isotopes are almost identical and correspond exactly to the previous experiment [30] which was carried out with much larger samples and, consequently, much better statistics. This agreement confirms that reliable data could also be obtained under the more difficult conditions of the present experiment.

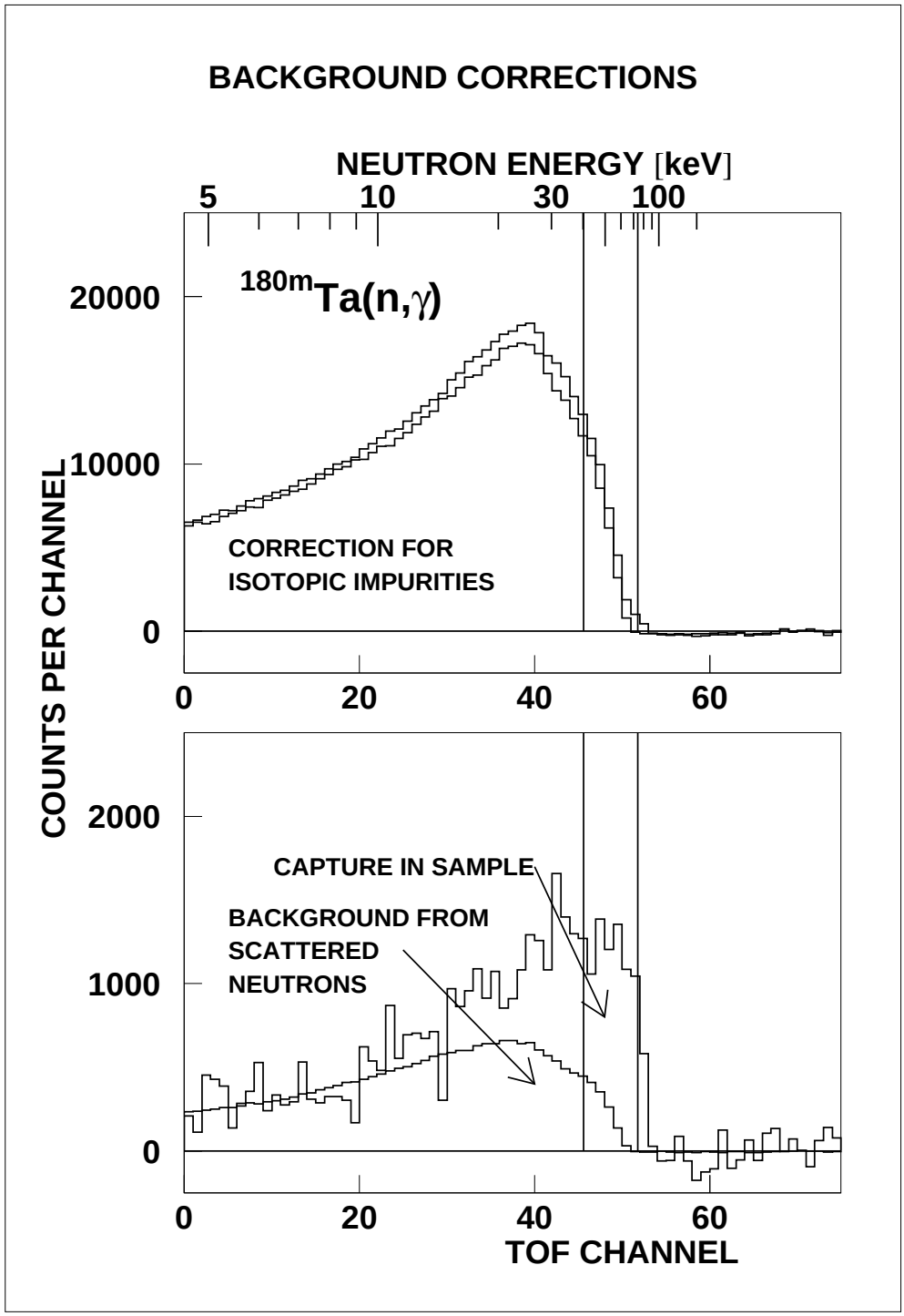

Figure 5: TOF spectrum of the ^{180m}Ta sample used for the determination of the cross section shape. The upper panel shows the spectrum corrected for sample independent background and the correction for isotopic impurities, and the lower panel shows the correction for capture of scattered neutrons. The original 2048 channel spectrum was rebinned into 128 channels. The region used for normalization of the cross section is indicated by vertical lines.

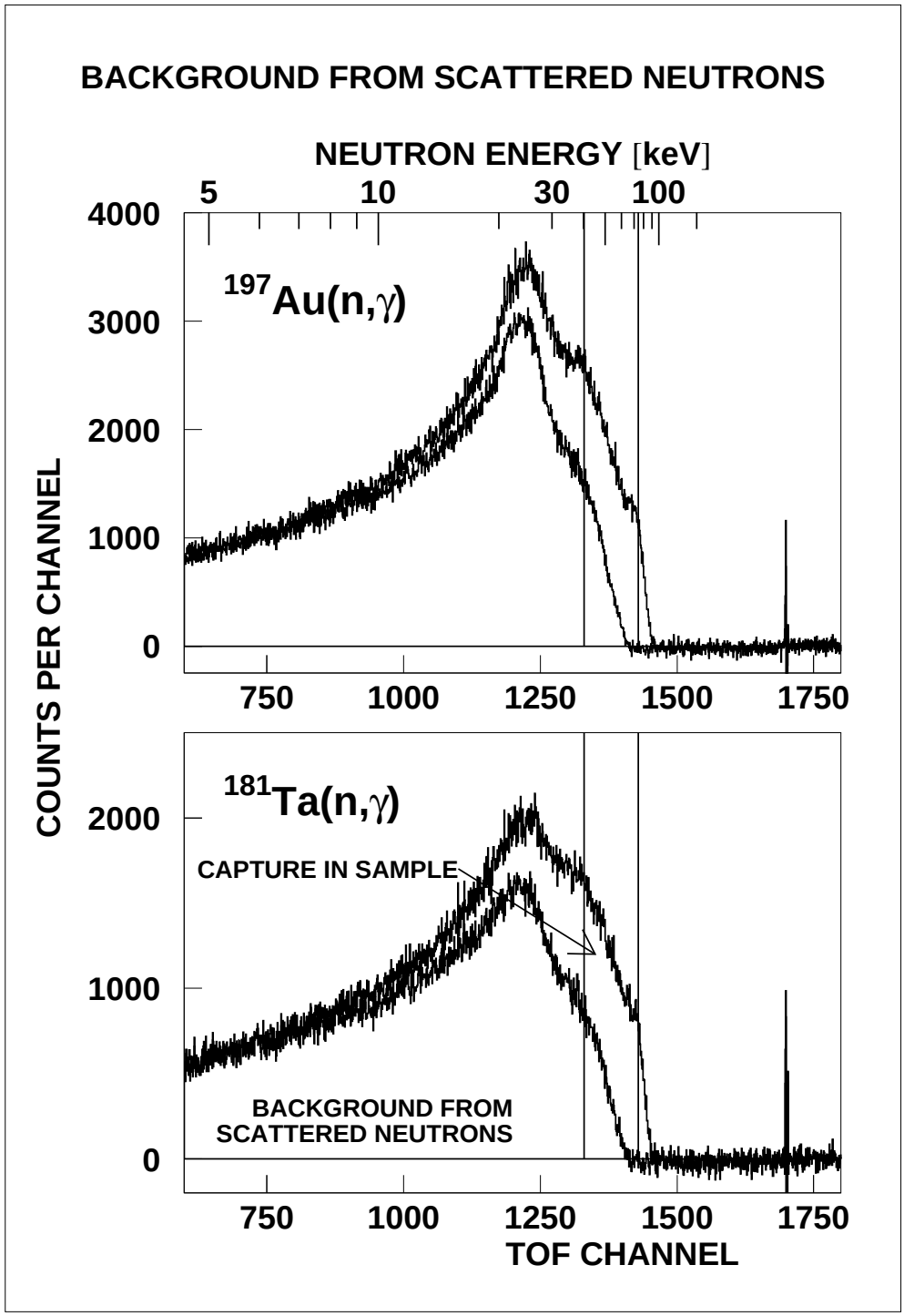

Figure 6: TOF spectra of the ^{197}Au and ^{181}Ta samples measured in run II with 80 keV maximum neutron energy. The background due to sample scattered neutrons is shown separately. The region for absolute normalization of the cross section is indicated by vertical lines.

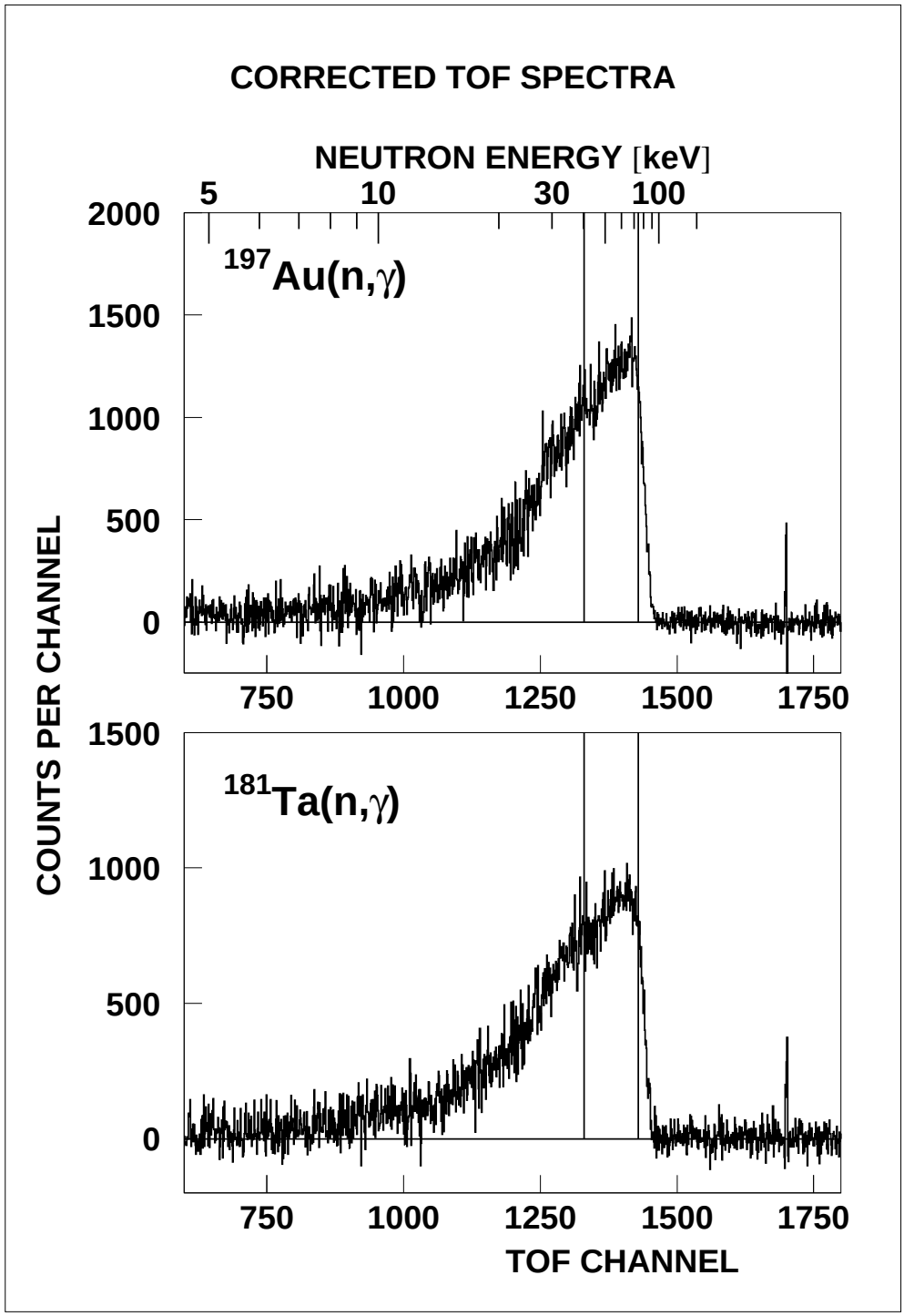

Figure 7: The background-corrected TOF spectra of the ^{197}Au and ^{181}Ta samples from run II used for the determination of the cross section shape. The region for absolute normalization of the cross section is indicated by vertical lines.

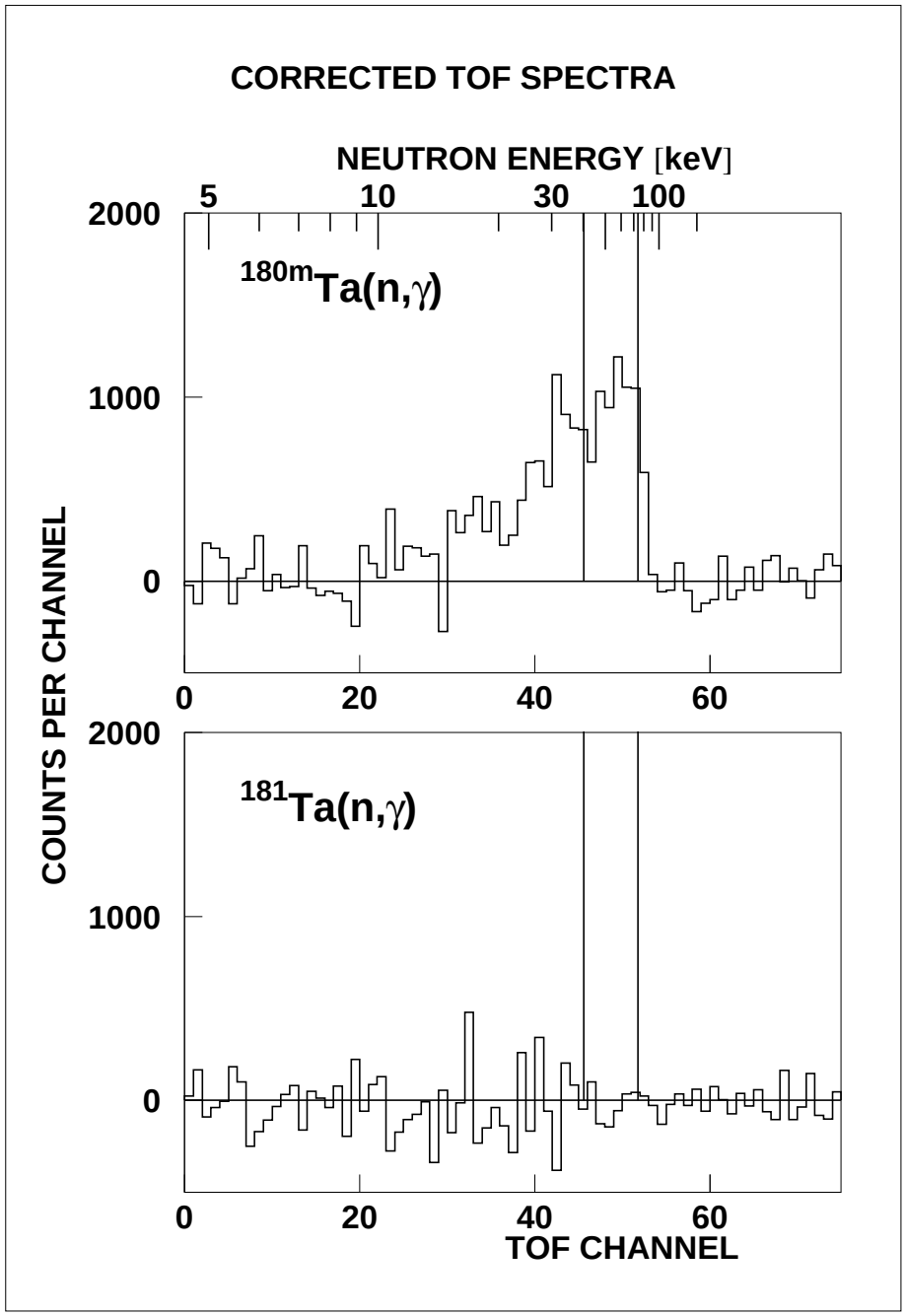

Figure 8: The background-corrected TOF spectrum of the ^{180m}Ta sample from run II (top panel). The counting statistics per channel was improved by rebinning the original 2048 channel spectrum into 128 channels. The region for absolute normalization of the cross section is indicated by vertical lines. The bottom panel shows the respective TOF spectrum measured with the natural tantalum sample integrated over the same sum energy range from 6.8 to 8 MeV (see Fig. 4). The absence of any time-correlated events illustrates the efficient background suppression via the sum energy information.

The TOF scale of the corresponding spectrum for the ^{180m}Ta sample (upper part of Fig. 8) is compressed by a factor 16 in order to reduce statistical fluctuations. In spite of

the comparably poor statistics it is evident that the spectrum shape equals that of the other samples. The lower part of Fig. 8 shows a projection using the same sum energy interval from 6.8 to 8 MeV (see Fig. 4) for the natural ^{181}Ta sample. There is clearly no indication for capture events, thus confirming the selectivity of the combined TOF and sum energy information.

3.2 Detection efficiency for capture events on ^{180m}Ta

For normalization, the two–dimensional data were projected onto the sum energy axis using the TOF region with optimum signal/background ratio indicated in Figs. 5 and 6 by vertical lines. The resulting sum energy spectra are shown in Fig. 9 for different multiplicities. These multiplicities correspond to the number of detector modules contributing per event, and are slightly larger than true multiplicities because of cross talking between modules. The arrows in Fig. 9 indicate the range of sum energy channels that were integrated to obtain the TOF spectra of Figs. 7 and 8 for determining the cross section shape.

The multiplicity distributions exhibit remarkable differences. Only 40% of the capture events in the ^{197}Au sample are observed with multiplicities $\geq$5, while the respective fraction in ^{181}Ta is about 50%. For ^{180m}Ta, however, 87$\pm$5% fall into this category, and only these events were used in further analysis. This fraction of ^{180m}Ta events was determined by means of a computer simulation as described below.

The final uncertainty of the measured ^{180m}Ta cross section is dominated by two components, by counting statistics and by the fraction of detected events. The integration of the sum energy spectrum from the experimental threshold at 1.7 MeV up to 8 MeV (bottom panels of Figs. 4 or 9), which is required for determining the absolute value of the cross section, is affected by large statistical uncertainties due to the backgrounds from the ^{181}Ta impurity (mainly at 6 to 7 MeV) and from natural radioactivities (up to 4 MeV). Since only events with multiplicities $\geq$5 could be recorded with sufficient signal/background ratio (Fig. 9), special efforts were required to determine this fraction reliably.

Therefore, the data were reanalyzed without applying the correction for isotopic impurities but only subtracting the background from scattered neutrons. This component was normalized in the usual way and eliminated the large background due neutrons scattered in the graphite container. The resulting spectra, which represent the sum of both experimental runs, are shown in Fig. 10 for the natural and the enriched tantalum sample.

The ^{180m}Ta and ^{181}Ta components in the spectrum of the enriched sample were separated by a fitting procedure [33] based on the previously measured sum energy spectra of about 20 isotopes covering a range of neutron separation energies between 4.78 MeV (^{232}Th) to 8.54 MeV (^{155}Gd). These spectra (which were not disturbed by capture to isomeric states) were approximated by a Gaussian for the full energy peak and a truncated polynomial for the low energy tail. The resulting parameter systematics allowed to characterize the intensity ratio of the full energy peak and the low energy part in a reliable way.

In the decomposition of the spectrum taken with the enriched sample (left panel of Fig. 10) the shape of the ^{181}Ta component was adopted from the spectrum of the natural sample (right panel of Fig. 10), whereas the ^{180m}Ta component was characterized by means

of the parameter systematics. Variation of the two remaining fit parameters (defining the height and width of the full energy peak) within the limits suggested by the systematics confirmed that the resulting ratio of the two spectrum components was quite stable.

The fit of the sum spectrum of the ^{180m}Ta sample in Fig. 11 showed that 81.5% of the observed events were due to captures on ^{181}Ta and 18.5% to captures on ^{180m}Ta. The fitted ^{180m}Ta component is compared in Fig. 12 with the spectrum obtained in the first evaluation, where the correction for isotopic impurities was directly subtracted. Since both methods were rather independent of each other the good agreement provides evidence for the reliability of the analysis.

The second important quantity is the fraction of capture events covered by the evaluated spectrum. This quantity was calculated by a full computer simulation of the experiment using the code GEANT [34], [35]. The geometry of the Karlsruhe $4\pi BaF_2$ detector was modeled for all 41 crystals including reflectors and other structural materials. The efficiency for γ-rays originating from a sample in the center of the detector was then calculated including the corrections for γ-ray self absorption and for conversion electrons. The energy resolution was taken from experimental information recorded with an ADC system.

Gamma-ray cascades from (n,γ) reactions on ^{180m}Ta, ^{181}Ta, and ^{197}Au were calculated using the CASINO version [36] of the Monte Carlo code DICEBOX [37] which is suited for the keV neutron energy range. An important feature of this code is the proper treatment of the probability for emission of conversion electrons. With these calculated γ-ray cascades the response of the $4\pi BaF_2$ detector was determined in the GEANT simulations by following the energy deposit in the individual modules down to the experimental threshold of $\sim$50 keV.

In this way the spectra measured by the individual modules as well as the sum-energy spectra of the full array were obtained for different cascade multiplicities as shown in Figs. 13 and 14 for ^{181}Ta and ^{180m}Ta, respectively. The amazing difference between the two cases observed in the experimental data is well reproduced in the GEANT calculations. While the average multiplicity of capture events on ^{181}Ta of 4.4 corresponds to the normal average for heavy nuclei, the respective value for ^{180m}Ta of 6.2 is the highest multiplicity ever measured with the Karlsruhe $4\pi BaF_2$ detector. The good agreement between simulation and experiment is illustrated in Figs. 15 and 16 where the calculated spectra are combined in the same way as the experimental results (see Fig. 9). For ^{181}Ta the direct comparison of simulated and measured spectra in Fig. 17 shows that even the spectral shape for different multiplicites is perfectly reproduced. Note that the calculated spectra are normalized to the experimental data only by a single number, namely by the integral from 1.7 to 8 MeV γ-ray energy in the total spectrum.

The excellent agreement between experiment and simulation confirms that capture events on ^{180m}Ta with multiplicity $\geq$5 are, indeed, detected with 83% efficiency, consistent with the 87$\pm$5% estimated directly from the measured spectra (see Fig. 9).

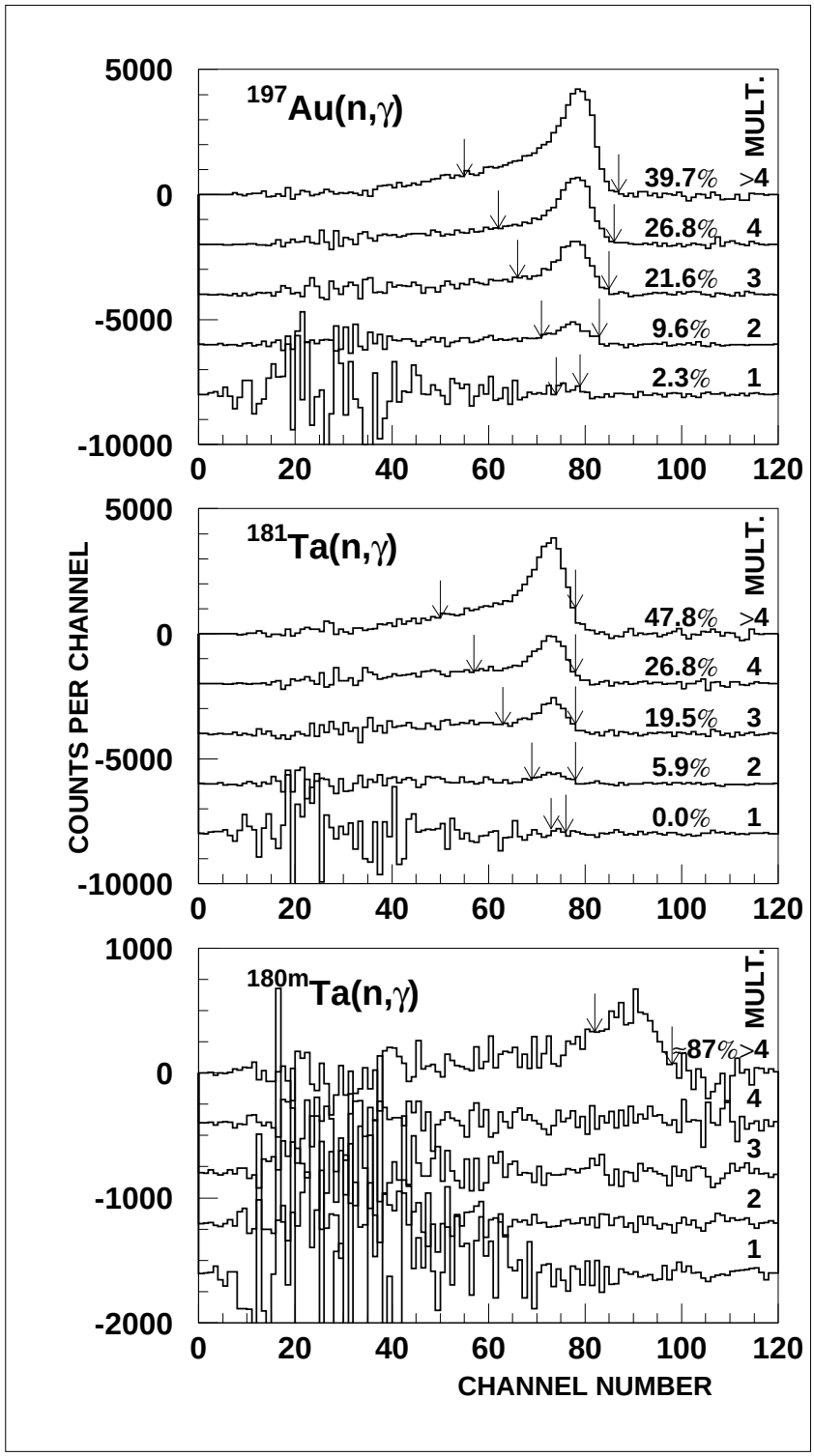

Figure 9: Sum energy spectra of all isotopes as a function of multiplicity. The regions used to determine the cross section shape (see Figs. 7 and 8) are indicated by arrows. For ^{180m}Ta only events with multiplicity $\geq$5 were used in the evaluation.

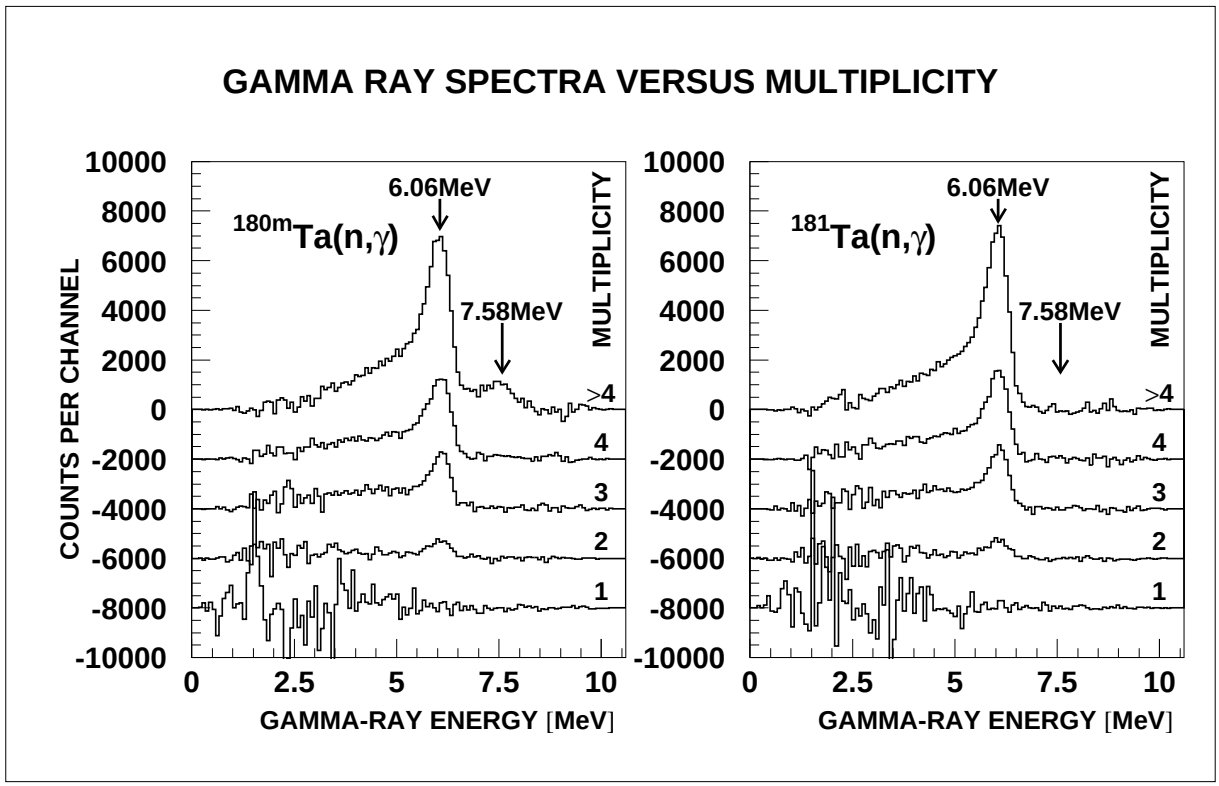

Figure 10: Sum energy spectra of both tantalum samples as a function of multiplicity. These spectra represent the data of both runs and were obtained without correction for isotopic impurities.

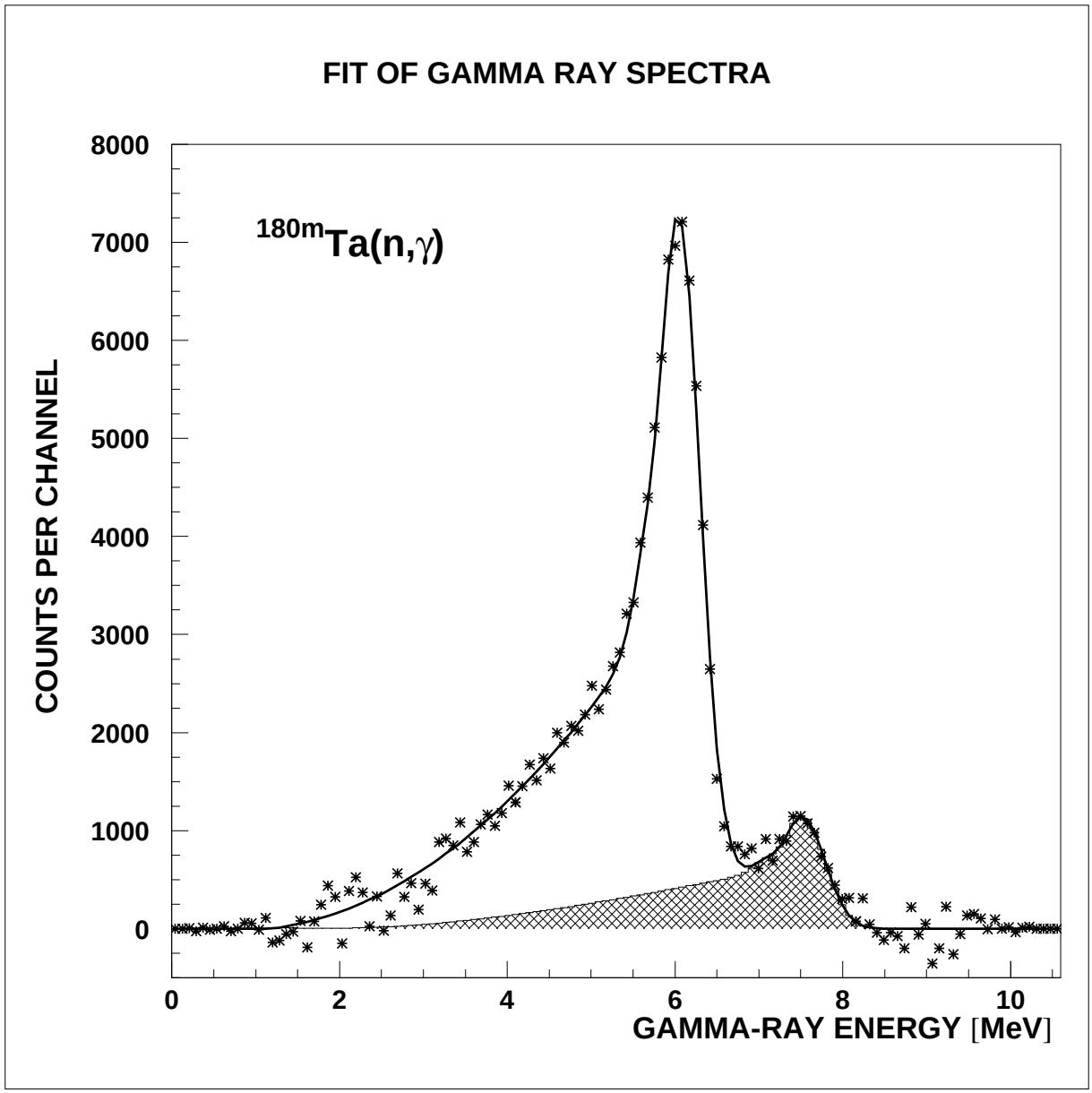

Figure 11: Sum energy spectrum of the enriched tantalum sample without correction for isotopic impurities (events with multiplicity ≥ 5 only, see Fig. 10). The two components are separated by a fitting procedure. The spectrum contains the data of both runs.

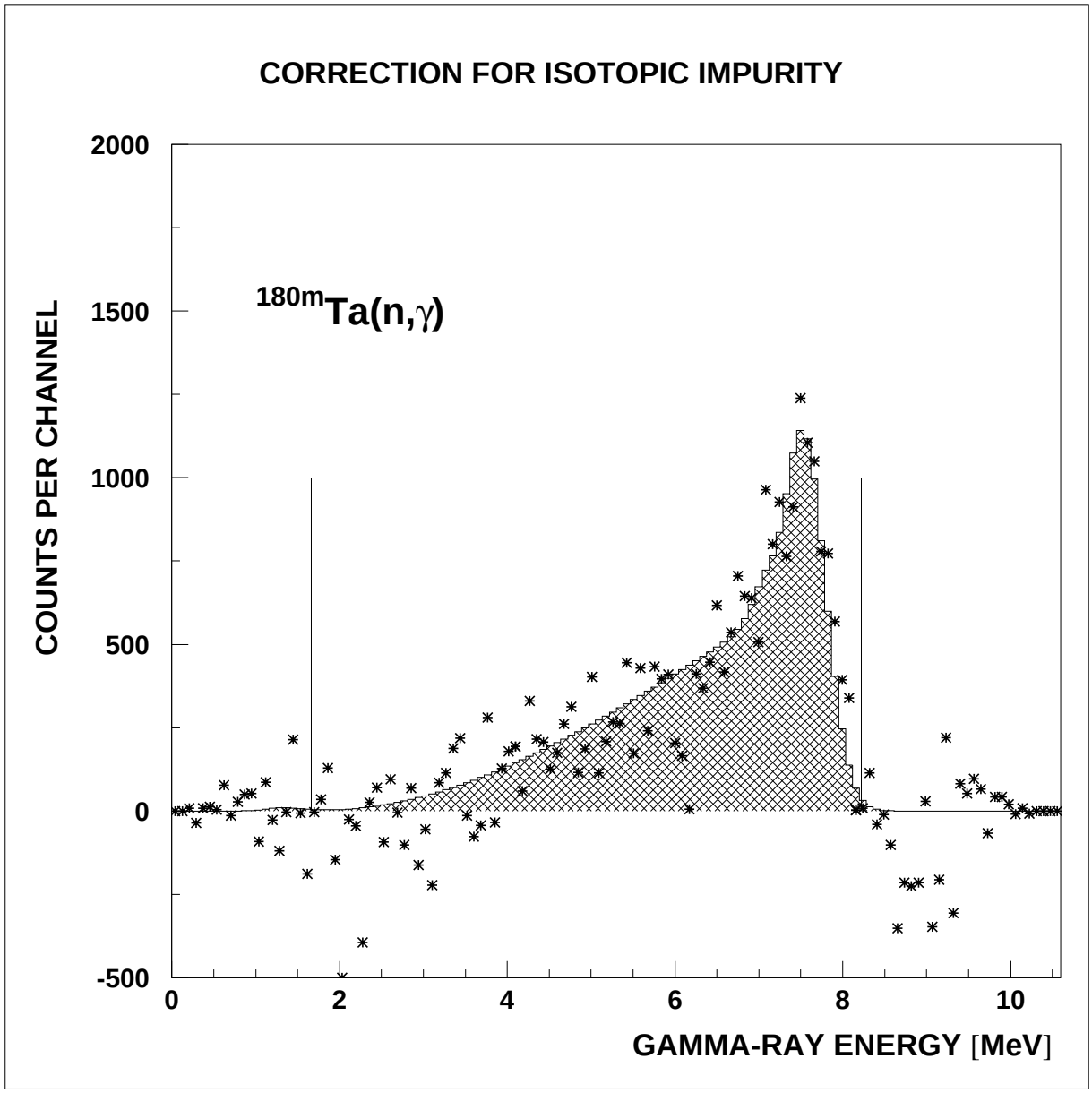

Figure 12: The fit to the spectrum evaluated without correction for isotopic impurities (hatched area) compared to the spectrum obtained including this correction. Note that the hatched area is the same as in Fig.11 and **not** a fit to the data.

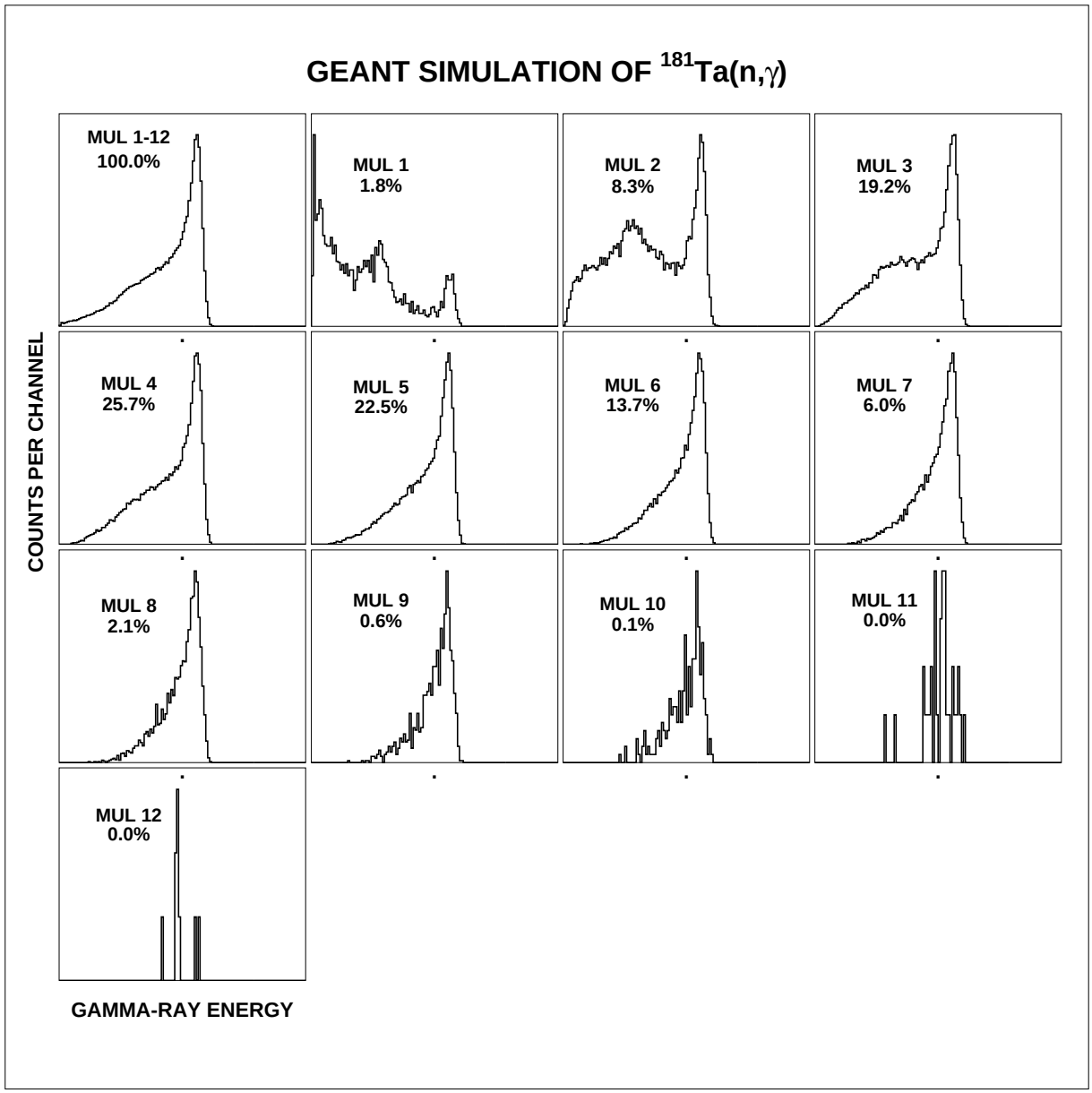

Figure 13: GEANT simulations of sum energy spectra versus detected event multiplicity based on theoretical γ-cascades for neutron capture on ^{181}Ta. Spectra for lower multiplicity exhibit significantly different shapes. The average multiplicity is 4.4.

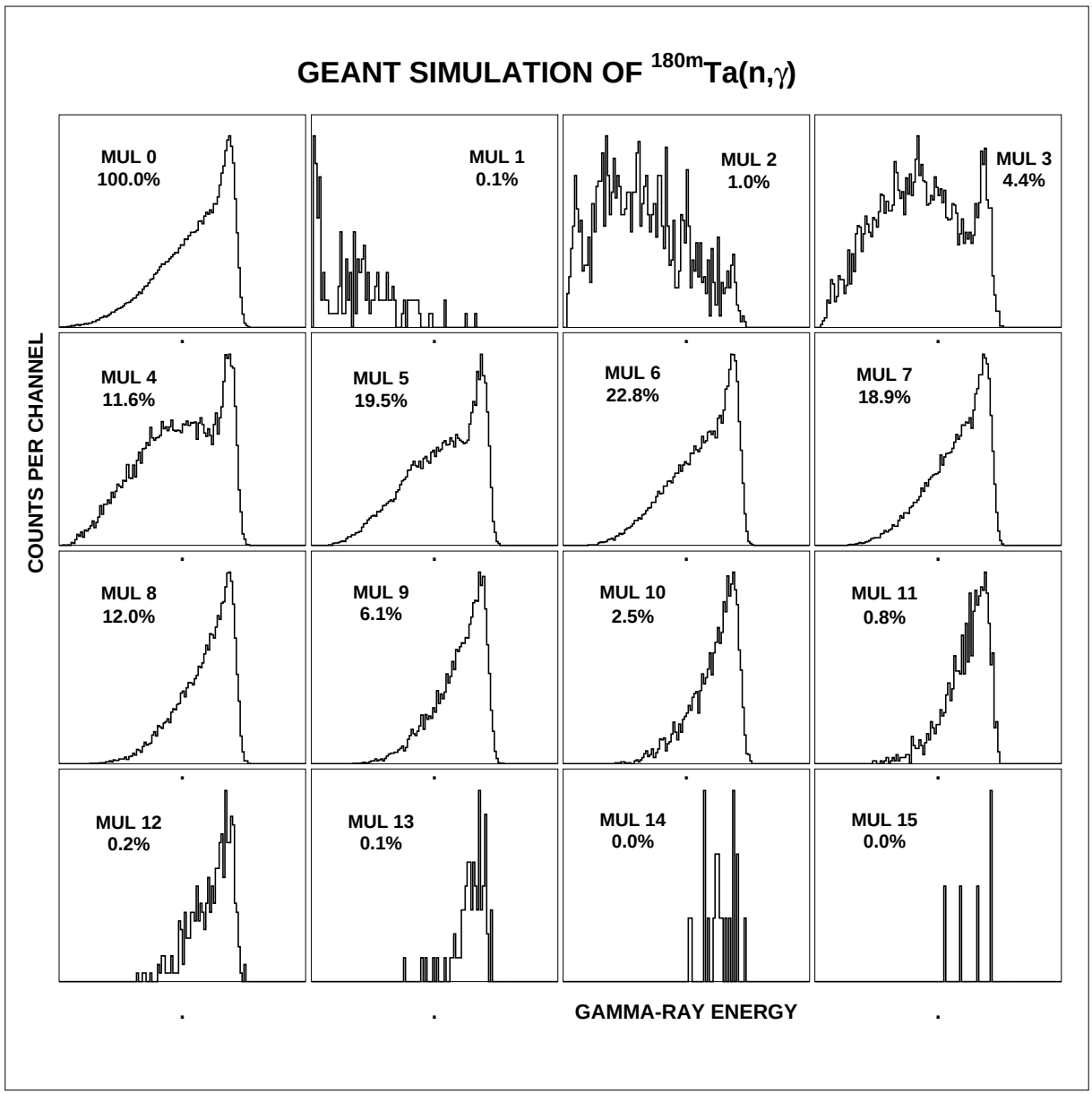

Figure 14: Same as Fig. 13 but for neutron capture on ^{180m}Ta. In this case, the average multiplicity of 6.2 is extraordinarily large.

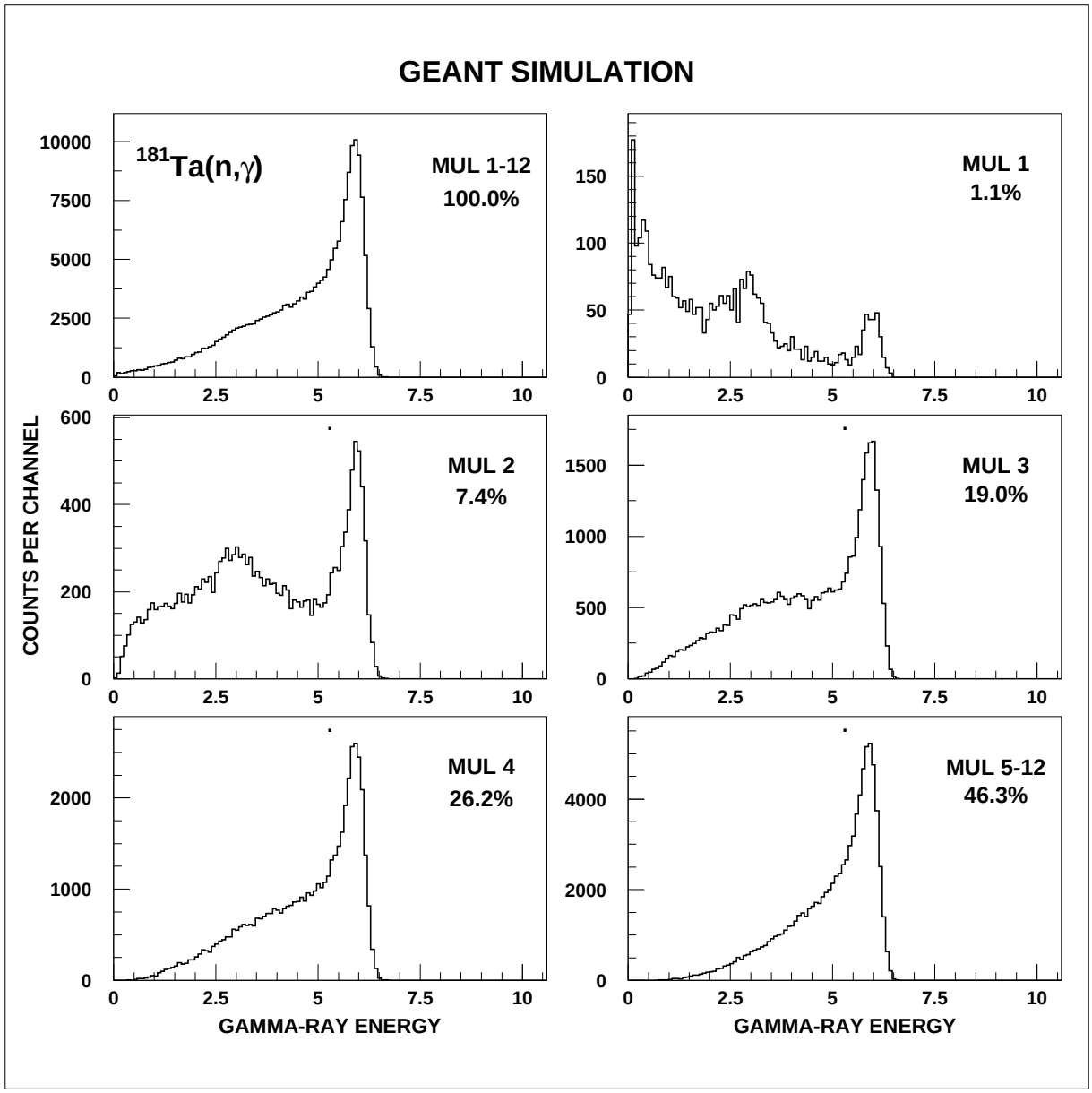

Figure 15: The spectra of Fig. 13 combined in the same way as the experimental data in Fig. 9. The measured contributions of the various multiplicities are well reproduced in the simulation.

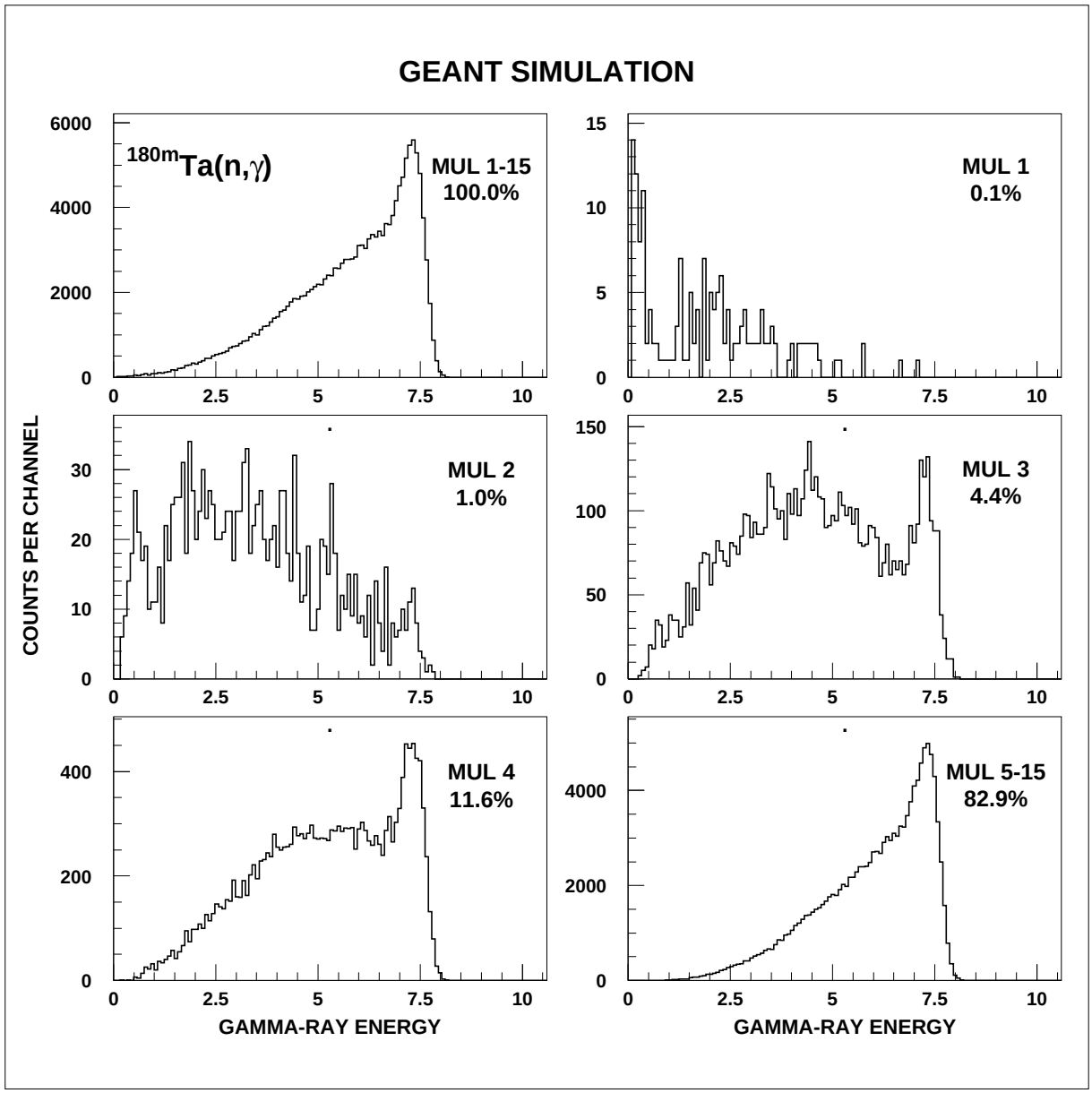

Figure 16: Same as Fig. 15 but for neutron capture on ^{180m}Ta. The 83% contribution of the spectrum with multiplicity $\geq$5 is in good agreement with the 87$\pm$5% directly estimated from the background-corrected spectrum in Fig. 9.

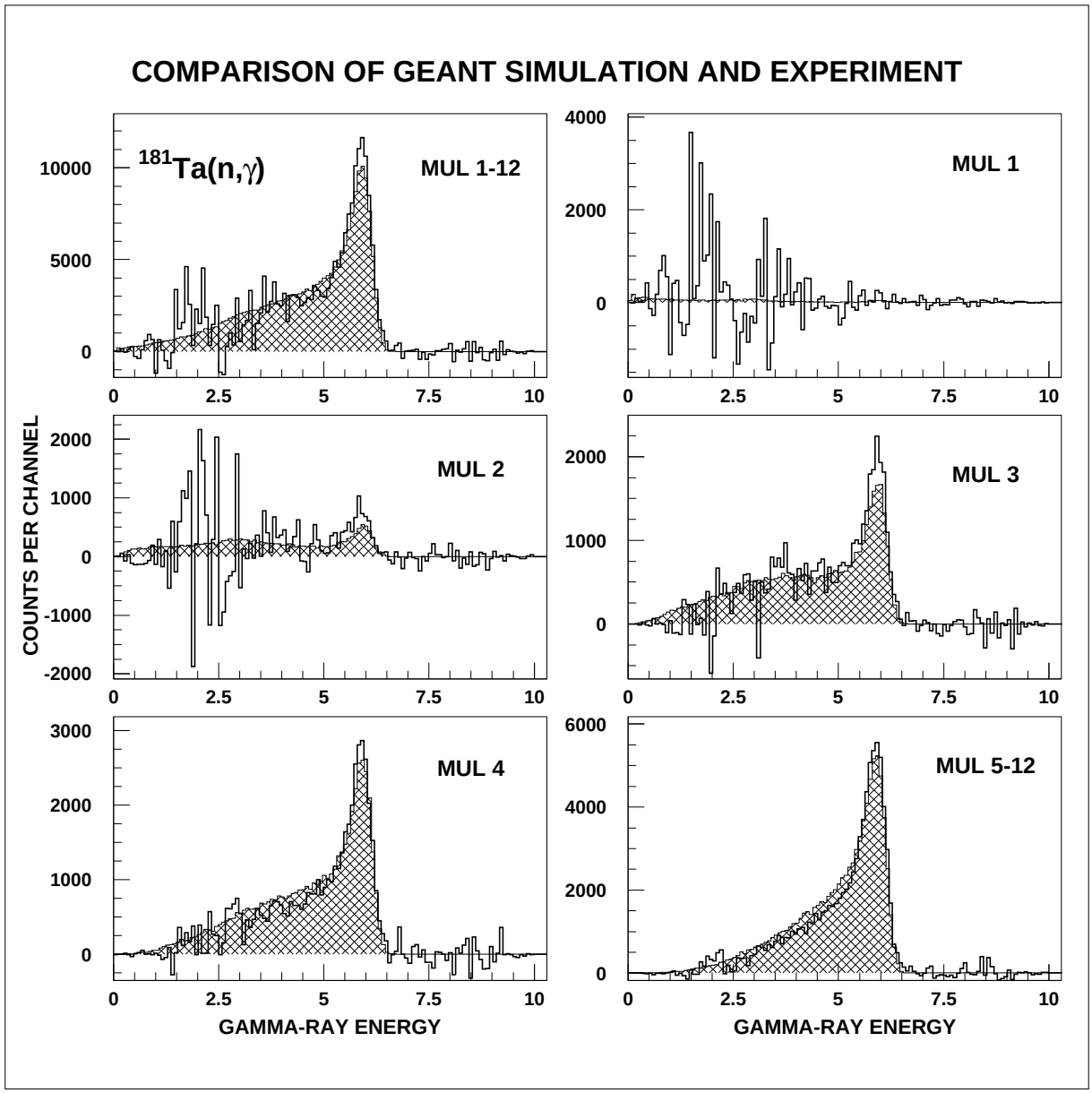

Figure 17: Comparison of the simulated spectra of Fig. 15 (dashed areas) and the measured spectra of Fig. 9 (histogram) illustrating that also the spectral shapes are well reproduced by the simulation.

3.3 Cross section ratios

The cross section ratio of isotope X relative to the gold standard is given by

$$\frac{\sigma_i(X)}{\sigma_i(Au)} = \frac{Z_i(X)}{Z_i(Au)} \cdot \frac{\Sigma Z(Au)}{\Sigma Z(X)} \cdot \frac{\Sigma E(X)}{\Sigma E(Au)} \cdot \frac{m(Au)}{m(X)} \cdot F_1 \cdot F_2 \qquad (1)$$

In this expression, Z_i is the count rate of channel i in the TOF spectrum, ΣZ is the TOF rate integrated over the interval used for normalization (indicated by the vertical lines in Figs. 7 and 8), ΣE is the total count rate in the sum energy spectra for all multiplicities in this TOF interval. The respective sum energy spectra are shown in Fig. 9. In case of ^{197}Au and ^{181}Ta these spectra were integrated for all multiplicities from the threshold at 1.7 MeV up to and slightly beyond the respective binding energy, and the corresponding sum, ΣE, was used in Eq. 1. (for a detailed discussion see Ref.[38]). For ^{180m}Ta, only the spectrum with multiplicity $\geq$5 could be analyzed as mentioned above, and ΣE was obtained by adopting the result of the GEANT simulation that this spectrum represents 82.9% of the total events (see Fig. 16).

The other quantities in Eq. 1 are the sample thickness m in atoms/barn, the correction $F_1 = (100 - f(Au))/(100 - f(X))$ which accounts for the undetected fraction of capture events f below the experimental threshold in sum energy, and F_2 is the ratio of the multiple scattering and self–shielding corrections. Index X refers to the respective tantalum sample.

The fraction of unobserved capture events, f, and the correction factor F_1 were calculated as described in Ref. [32]. The input for this calculation are the detector efficiency for monoenergetic γ–rays in the energy range up to 10 MeV and the capture γ–ray cascades as used in the GEANT simulations. In case of gold the capture cascades were calculated with various sets of input parameters. The main difference in these calculations was that for describing the decay of the compound nucleus in some cases a pygmy resonance was considered in addition to the giant dipole resonance. Since the experimentally determined capture cascades were better reproduced, the data sets based on the pygmy resonance were adopted in the final analysis. On average the absolute f-values for the gold sample agree to 0.3% with results based on calculated cascades of G. Reffo and M. Uhl that had been used in Ref. [39].

The correction factors F_1 are quoted in Table 3. There is remarkable agreement (within 1.6%) compared to the F_1 values calculated for the first tantalum measurement with the Karlsruhe 4πBaF$_2$ detector [32]. Meanwhile, the solid angle of the detector array was improved from 94% to 96%, and the calculated efficiency for monoenergetic γ-rays was replaced by measured data. Note that the f-values for ^{180m}Ta are fairly small: the detection efficiency for this isotope is nearly 100% due to the large cascade multiplicity.

The corrections for neutron multiple scattering and self–shielding could be neglected since the sample masses were $\sim$8 times smaller than in the previous measurement on natural tantalum [32] where this correction was $\sim$1% in the neutron energy range considered here.

Table 3: FRACTION f OF UNDETECTED CAPTURE EVENTS (in %) AND THE RELATED CORRECTION FACTORS F_1.[a]

	Threshold in Sum Energy (MeV)		
	1.5	1.7	2.0
f(Au)	4.36		6.27
$f(^{180m}\mathrm{Ta})$	0.35		0.85
$f(^{181}\mathrm{Ta})$	1.76		3.11
$F_1(^{180m}\mathrm{Ta/Au})$	0.960	0.954	0.945
$F_1(^{181}\mathrm{Ta/Au})$	0.974	0.971	0.967

[a] Derived from capture cascades calculated with the code CASINO [36].

4 RESULTS FOR THE NEUTRON CAPTURE CROSS SECTIONS

The measured neutron capture cross section ratios of ^{180m}Ta, ^{181}Ta, and of ^{197}Au are listed in Tables 4 and 5 together with the respective statistical uncertainties. The data are given for each of the two runs and for the two evaluation methods separately. The last column in each table contains the weighted average, the weight being determined by the inverse of the squared statistical uncertainties. Since the cross section ratios depend weakly on energy, the averages for the energy interval from 30 to 80 keV are also included for a better comparison of the individual results. The data are free of systematic differences with respect to different runs or evaluations, thus confirming the consistent treatment of the respective data sets which were characterized by different experimental conditions, e.g. with respect to neutron spectra and signal/background ratios.

As in previous measurements with the 4π BaF_2 detector [29, 30, 40] the final cross section ratios were adopted from evaluation 2. The respective mean values are compiled in Table 6 together with the statistical, systematic, and total uncertainties. The energy bins are sufficiently fine to avoid systematic uncertainties in the calculation of the Maxwellian averaged cross sections (Sec. 6). In the energy range from 30 to 100 keV the uncertainties of the cross section ratios are $\sim$10% for ^{180m}Ta and $\sim$2% for ^{181}Ta, but increase significantly at lower energies.

The experimental ratios were converted into absolute cross sections using the gold data of Macklin [41] after normalization by a factor of 0.989 to the absolute value of Ratynski and Käppeler [42] (Table 7). The uncertainties of the resulting values can be obtained by adding the 1.5% uncertainty of the reference cross section to the uncertainties of the respective cross section ratios.

The present results are compared to previous data in Figs. 18 and 19. Since there

are no other experimental data for ^{180m}Ta this comparison is restricted to the available calculated data sets. It is important to note that all calculations overestimate the ^{180m}Ta cross section significantly. Obviously, statictical model calculations can be rather uncertain even for nuclei with high level densities. The calculations by Németh et al. [6] and Rauscher and Thielemann [43], which are based on local and global parameter systematics, respectively, yield nearly a factor of two larger cross sections compared to the experiment. In the calculation of Beer and Macklin [15] average radiation widths and level spacings deduced from data at thermal neutron energies were included [44, 45], leading to a smaller discrepancy of about 30%.

The results for ^{181}Ta are in very good agreement with the cross sections obtained in the first experiment with the Karlsruhe 4πBaF$_2$ detector [32]. Since the previous measurement was performed with an eight times larger metallic sample without any additional container, the agreement with the present results confirms that the significant background due to scattered neutrons from the sample container was properly corrected.

Table 4: CROSS SECTION RATIOS $\sigma(^{180m}\mathrm{Ta})/\sigma(^{197}\mathrm{Au})$ AND STATISTICAL UNCERTAINTIES (in %)

Energy Bin (keV)	Run I		Run II		Average	
Evaluation 1						
10 – 12.5	–	–	4.19	38.	4.19	38.
12.5 – 15	2.45	78.	2.20	57.	2.29	46.
15 – 20	2.76	38.	4.06	20.	3.79	18.
20 – 25	3.59	24.	2.89	23.	3.22	17.
25 – 30	2.30	27.	2.73	18.	2.59	15.
30 – 40	2.64	16.	3.09	12.	2.94	9.5
40 – 50	2.40	17.	2.55	11.	2.50	9.2
50 – 60	3.26	12.	2.51	10.	2.81	8.0
60 – 80	2.58	9.4	2.51	9.1	2.54	6.5
80 – 100	2.72	8.3	1.83	46.	2.69	8.2
30 – 80	2.72	6.6	2.67	8.1	2.70	5.1
Evaluation 2						
10 – 12.5	–	–	3.54	39.	3.54	39.
12.5 – 15	1.71	99.	1.42	89.	1.55	67.
15 – 20	1.84	56.	3.93	20.	3.70	19.
20 – 25	4.14	21.	2.32	26.	3.39	17.
25 – 30	2.44	27.	2.54	18.	2.51	15.
30 – 40	2.80	15.	2.91	11.	2.87	9.1
40 – 50	2.19	18.	2.44	11.	2.38	9.1
50 – 60	3.03	13.	2.61	9.5	2.76	7.6
60 – 80	2.44	9.8	2.56	8.5	2.51	6.4
80 – 100	2.76	8.2	1.69	44.	2.73	8.1
30 – 80	2.62	6.8	2.63	7.5	2.63	5.0

Table 5: CROSS SECTION RATIOS $\sigma(^{181}\mathrm{Ta})/\sigma(^{197}\mathrm{Au})$ AND STATISTICAL UNCERTAINTIES (in %)

Energy Bin (keV)	Run I		Run II		Average	
Evaluation 1						
10 – 12.5	1.2130	17.	1.3993	11.	1.3425	9.1
12.5 – 15	1.6310	13.	1.2830	9.4	1.4067	7.6
15 – 20	1.1777	8.6	1.2993	5.9	1.2605	4.9
20 – 25	1.3761	6.5	1.4018	5.2	1.3917	4.1
25 – 30	1.3351	5.1	1.3740	4.3	1.3579	3.3
30 – 40	1.3083	3.7	1.3031	3.4	1.3055	2.5
40 – 50	1.3464	3.6	1.2570	3.3	1.2977	2.4
50 – 60	1.3062	3.5	1.2519	3.2	1.2769	2.4
60 – 80	1.2882	2.8	1.2163	3.1	1.2562	2.1
80 – 100	1.2818	2.7	1.1974	9.0	1.2747	2.6
30 – 80	1.3123	2.4	1.2571	2.9	1.2841	1.8
Evaluation 2						
10 – 12.5	1.3018	10.	1.3294	7.7	1.3195	6.2
12.5 – 15	1.5108	10.	1.3913	7.0	1.4299	5.7
15 – 20	1.2452	6.4	1.4480	4.1	1.3897	3.4
20 – 25	1.4871	5.0	1.4171	3.6	1.4405	2.9
25 – 30	1.4197	4.2	1.3408	2.8	1.3658	2.4
30 – 40	1.3470	3.1	1.3189	2.1	1.3274	1.7
40 – 50	1.3394	3.1	1.2802	1.9	1.2968	1.6
50 – 60	1.2948	3.0	1.2529	1.9	1.2647	1.6
60 – 80	1.2920	2.6	1.2263	1.8	1.2473	1.4
80 – 100	1.2677	2.5	1.1517	6.5	1.2523	2.4
30 – 80	1.3183	2.3	1.2696	1.5	1.2841	1.3

Table 6: FINAL NEUTRON CAPTURE CROSS SECTION RATIOS OF ^{180m}Ta AND ^{181}Ta RELATIVE TO ^{197}Au

Energy Bin[a]	$\frac{\sigma(^{180m}Ta)}{\sigma(^{197}Au)}$	Uncertainty (%)			$\frac{\sigma(^{181}Ta)}{\sigma(^{197}Au)}$	Uncertainty (%)		
(keV)		stat	sys	tot		stat	sys	tot
10 – 12.5	3.54	39.	5.1	39.	1.3195	6.2	0.5	6.2
12.5 – 15	1.55	67.	5.1	67.	1.4299	5.7	0.5	5.7
15 – 20	3.70	19.	5.1	20.	1.3897	3.4	0.5	3.4
20 – 25	3.39	17.	5.1	18.	1.4405	2.9	0.5	2.9
25 – 30	2.51	15.	5.1	16.	1.3658	2.4	0.5	2.5
30 – 40	2.87	9.1	5.1	10.	1.3274	1.7	0.5	1.8
40 – 50	2.38	9.1	5.1	10.	1.2968	1.6	0.5	1.7
50 – 60	2.76	7.6	5.1	9.2	1.2647	1.6	0.5	1.7
60 – 80	2.51	6.4	5.1	8.2	1.2473	1.4	0.5	1.5
80 – 100	2.73	8.1	5.1	9.6	1.2523	2.4	0.5	2.5

[a] Energy bins as used for calculating the Maxwellian averaged cross section

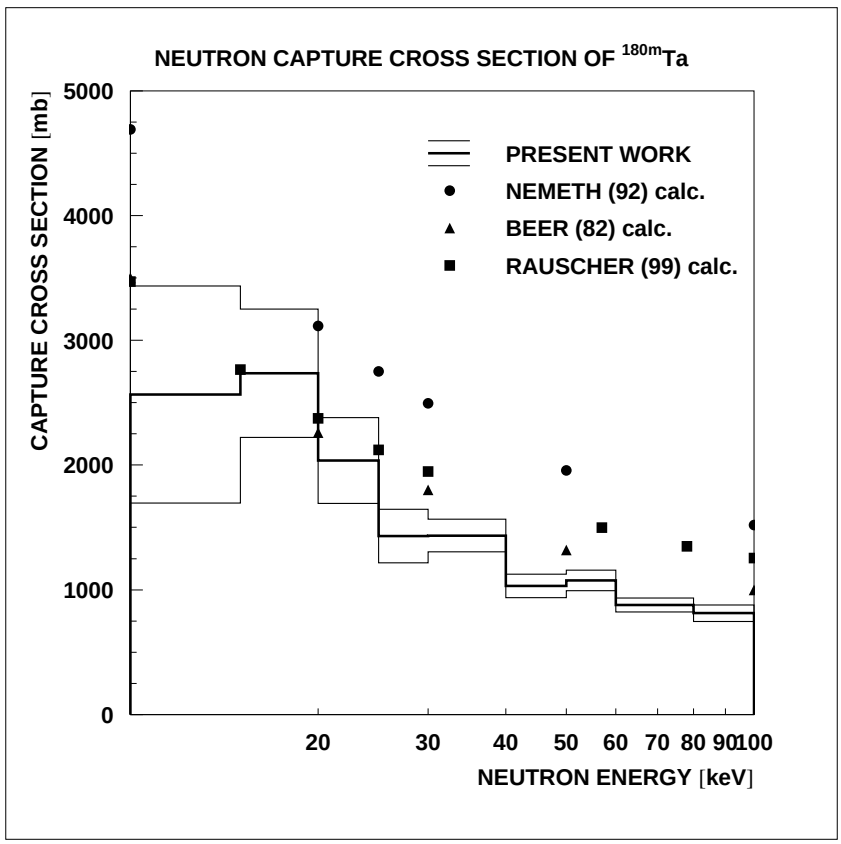

Figure 18: The neutron capture cross section of ^{180m}Ta compared to previous calculations [6, 15, 43].

Table 7: NEUTRON CAPTURE CROSS SECTIONS OF ^{180m}Ta AND ^{181}Ta (in mb)

Energy Bin[a] (keV)	$\sigma(^{197}\mathrm{Au})^b$	$\sigma(^{180m}\mathrm{Ta})$	$\sigma(^{181}\mathrm{Ta})$
10 – 12.5	1066.7	3772.	1408.
12.5 – 15	878.0	1360.	1255.
15 – 20	738.8	2736.	1027.
20 – 25	600.0	2036.	864.3
25 – 30	570.8	1431.	779.6
30 – 40	500.4	1435.	664.2
40 – 50	433.3	1032.	562.0
50 – 60	389.6	1076.	492.8
60 – 80	349.4	877.0	435.8
80 – 100	298.3	813.4	373.6

[a] As used for calculating the Maxwellian averaged cross sections
[b] Based on the ^{197}Au data from literature [41, 42]

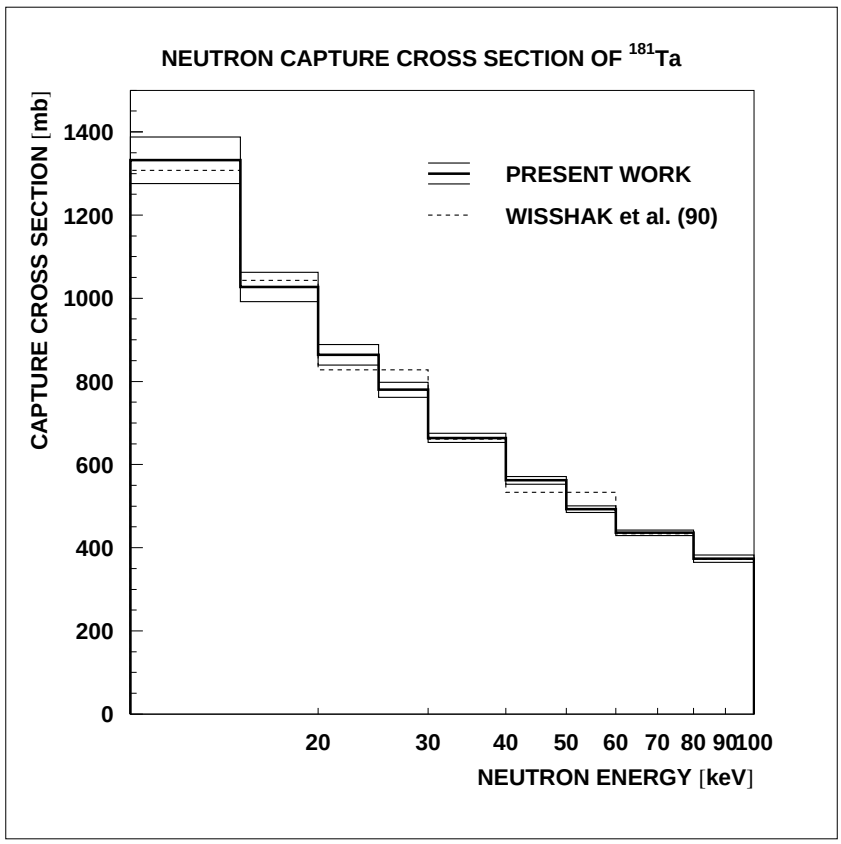

Figure 19: The neutron capture cross section of ^{181}Ta compared to the previous measurement with the Karlsruhe 4πBaF$_2$ detector [32].

5 DISCUSSION OF UNCERTAINTIES

The determination of statistical and systematic uncertainties in measurements with the 4π BaF_2 detector has been described in Refs. [29, 30, 32]. The following discussion emphasizes the particular aspects of the present experiment. The various uncertainties are summarized in Table 8.

The binding energy for all investigated isotopes is sufficiently low for normalizing the scattering background in the sum energy region around 9 MeV. This is essential for the present experiment since this background is unusually large due to the graphite sample container (see Figs. 5 and 6). In particular, it was found important that the significant TOF dependence of this correction could be considered. The absence of systematic differences in the data obtained in individual runs (see Tables 4 to 5) implies that systematic uncertainties were well under control, similar to previous measurements [29, 39, 46]. This is also confirmed by the agreement with the ^{181}Ta cross section of the first experiment [32], especially at low energies where the signal/background ratio is most crucial.

The systematic uncertainties related to the flight path and the neutron flux normalization have been discussed previously and are given in Table 8.

In the chemical analysis of the ^{180m}Ta sample, measurable impurities were only found for Na and Si with abundances of 0.01%. For all other elements upper limits in the range from 0.02 to 0.05% were obtained. Since the most critical europium impurity was even below 0.005%, a systematic uncertainty of 0.5% could be assumed for neglecting the corrections for chemical impurities. In case of the natural tantalum oxyde this uncertainty was only 0.1%.

The isotopic composition of the ^{180m}Ta sample (Table 1) was specified with an absolute uncertainty of <0.05%. Accordingly, a correlated uncertainty of 0.1% was assumed for the sample mass.

The evaluation of the uncertainty related to the isotopic correction has been described for the gadolinium and dysprosium isotopes [39, 46]. Following this discussion, this uncertainty can be estimated by the total count rates below 6.5 MeV (see Figs. 11 and 12). The subtracted rate due to the isotopic correction being 100000 compared to the remaining 25000 true events relates with the uncertainty of 0.05% for the isotopic composition to yield a total uncertainty of 0.2% for the isotopic correction.

The correction for multiple scattering and self-shielding was negligible due to the low sample mass. A corresponding uncertainty of 0.2% was adopted under the assumption that the graphite container affected the count rates of the tantalum and gold samples in the same way.

The systematic uncertainties due to undetected events were discussed in detail for the gadolinium experiment [39], where uncertainties of 0.3% for the even and 0.8% for the odd isotopes were estimated for the correction factor F_1. This estimate was based on two independent sets of calculated capture cascades, and was found to agree with the respective uncertainties quoted in previous measurements with the 4π BaF_2 detector

[29, 30, 40]. It turned out that this uncertainty was mainly determined by the difference in binding energy between the investigated isotope and the gold standard, which is large for the odd, but small for the even gadolinium isotopes. For ytterbium the same effect was observed [33]. However, the differences are slightly larger for the even and lower for the odd isotopes, with different signs for odd and even nuclei. Therefore, uncertainties of 0.4% and 0.7% were assigned, respectively, similar to the dysprosium isotopes [46]. According to this discussion, uncertainties of 0.6% and 0.4% are obtained for ^{180m}Ta and ^{181}Ta, respectively.

Compared to previous measurements with the 4π BaF_2 detector two additional systematic uncertainties had to be considered in the ^{180m}Ta analysis since it was based on events with multiplicity $m \geq 5$ only. These contributions, which refer to the efficiency for detecting $m \geq 5$ events and to the relative probability for such events, are completely dominating the overall systematic uncertainty.

The efficiency for detecting $m \geq 5$ events in neutron captures on ^{180m}Ta was determined in two ways (Sec. 4), first by applying the full correction for the ^{181}Ta impurity and integrating the count rate from threshold at 1.7 MeV to the sum energy peak. In addition, the ^{181}Ta and ^{180m}Ta components in the spectrum were separated by a fitting procedure derived from the systematics of sum energy spectra measured in previous experiments. The results obtained by this second procedure differed systematically by 5%. Therefore, a systematic uncertainty of 3% was assumed for the finally adopted average of the two results.

The relative probability for $m \geq 5$ events was first determined from the experimental spectra to be 87$\pm$5 % as shown in Fig. 9, whereas the detailed simulation of the experiment with the code GEANT yielded a value of 82.9% (see Fig.16). Since the experimental data for capture on ^{181}Ta were almost perfectly reproduced by the respective simulation, the related uncertainty was estimated to be 4%.

All systematic uncertainties are summarized in Table 8. In contrast to previous studies, the comparably small samples used in the present imply that the overall uncertainty is governed by counting statistics (Table 6).

6 MAXWELLIAN AVERAGED CROSS SECTIONS

Maxwellian averaged cross sections were calculated in the same way as described in Refs. [30, 32]. The neutron energy range from 0 to 700 keV was divided into three intervals according to the origin of the adopted cross sections. The respective contributions I_x are given in Table 9.

The interval I_2 from 20 to 100 keV, which corresponds to the energy range of this experiment (Table 7), contributes $\sim$60% to the Maxwellian averaged cross section at kT=30 keV. The contributions I_1 and I_3 listed in Table 9 were determined from the mean of the calculated cross sections of Németh et al. [6], of Beer and Macklin [15], and of Rauscher and Thielemann [43]. These calculated data sets were normalized to the present results in the neutron energy range from 20 to 80 keV, and their relative

Table 8: SYSTEMATIC UNCERTAINTIES (%)

Flight path	0.1
Neutron flux normalization	0.2
Sample mass:	
elemental impurities (^{180m}Ta/^{181}Ta)	0.5/0.1
isotopic composition (^{180m}Ta)	0.1
Isotopic correction (^{180m}Ta)	0.2
Multiple scattering and self–shielding: F_2	
cross section ratio (^{180m}Ta/^{181}Ta)	0.2
Undetected events: F_1	
cross section ratio (^{180m}Ta/^{181}Ta)	0.6/0.4
Number of events with multiplicity $\geq$5 (^{180m}Ta)	3.0
Percentage of events with multiplicity $\geq$5 (^{180m}Ta)	4.0
total systematic uncertainties	
$\sigma(^{180m}\mathrm{Ta})/\sigma(\mathrm{Au})$	5.1
$\sigma(^{181}\mathrm{Ta})/\sigma(\mathrm{Au})$	0.5

differences were used to derive the corresponding uncertainties.

The overall systematic uncertainties of the Maxwellian averaged cross sections in Table 9 include the uncertainties of the cross section ratios (Table 6) and of the extrapolated components, I_1 and I_3. The 1.5% uncertainty of the gold standard was not included since it cancels out in most applications of relevance for s–process studies.

Since other experimental data are not available, the present results for kT=30 keV thermal energy are eventually compared in Table 10 with previous calculations and with the compilations of Bao and Käppeler [47] and Bao et al. [48]. The severe discrepancies between the present result and the previous calculations have been noted already for the energy dependent cross sections and are also reflected in the Maxwellian averages. The recommended value of the recent compilation by Bao et al. [48], which is in fair agreement with the experiment, is not based on calculations but rather on the systematics of measured cross sections in the mass 180 region.

Table 9: MAXWELLIAN AVERAGED NEUTRON CAPTURE CROSS SECTION OF ^{180m}Ta

ΔE	0 - 20 keV	20 - 100 keV	100 - 700 keV	Thermal Spectrum			
kT	I_1, see text	I_2, this work	I_3, see text	$<\sigma v>/v_T$ (mbarn)			
(keV)	(mbarn)	(mbarn)	(mbarn)		stat	sys[a]	tot
8	2550±178	509.±50	0.	3059	185	156	242
10	2009±140	686.±61	0.	2695	153	137	205
15	1211±84	926.±70	6.0±0.3	2143	109	109	154
20	803±56	992.±68	29±1.5	1824	88	93	128
25	569±40	974.±63	70±3.5	1613	75	82	111
30	424±30	920.±58	121±6.1	1465	66	75	100
40	261±18.	781.±47	227±11	1269	52	65	83
50	176±12	650.±38	319±16	1145	43	58	72
52	165±12	626.±37	334±17	1125	42	57	71
60	127±8.9	541.±32	390±20	1058	39	54	67
70	958±6.7	454.±26	443±22	993	35	51	62
80	749±5.2	385.±22	482±24	942	33	48	58
90	601±4.2	330.±19	510±26	900	32	46	56
100	493±3.5	285.±16	529±26	863	31	44	54

[a]The 1.5% uncertainty of the gold standard is not included here, since it cancels out in most applications of relevance for nuclear astrophysics.

Table 10: MAXWELLIAN AVERAGED CROSS SECTION OF ^{180m}Ta (in mb) AT kT=30 keV COMPARED TO PREVIOUS CALCULATIONS AND EVALUATIONS

This Work	Previous Calculations		Evaluations	
1465±100[a]	2355	1999, Ref. [43]	1800±200	1987, Ref. [47]
	2662±530	1992, Ref. [6]	1640±260	2000, Ref. [48]
	1800±200	1982, Ref. [15]		

[a] The 1.5% uncertainty of the gold cross section is not included, since it cancels out in most applications of relevance for nuclear astrophysics.

7 THE s-PROCESS YIELD OF ^{180m}Ta

Based on the previously available data, the analysis of Arlandini et al. [19] found a 17% overproduction of ^{180m}Ta with the classical approach, while for the stellar model the s process accounted for $\sim$ 50% of the solar abundance. In the latter case the two branchings feeding the ^{180m}Ta had approximatively the same importance. The difference to the classical model was easily explained in terms of the higher temperature of that approach, which favored the β^- decay of ^{179}Hf [49].

Even larger differences between the two models were obtained for the closely related ^{180}W yields. Because the branching is not activated during the ^{13}C(α,n)^{16}O neutron burst, the stellar model found a 5% production for this nucleus. In the classical model this production is more prolific, resulting in an s-process contribution of more than 80%. However, recent p-process calculations reported also a significant production for this nucleus, from 50% [25] to 100% [27, 50]. If these yields are considered as well, the resulting overproduction exceeds by far the 15% limit allowed by the uncertainty of the empirical product of stellar cross section and solar abundance, which characterizes the s abundance in the classical approach.

This situation changed after the photoactivation experiment of Belic *et al.* [17] which demonstrated that ^{180}Ta is completely thermalized at kT = 30 keV, resulting in a total destruction in the constant temperature scenario assumed by the classical s-process approach. Concomitant with the destruction of ^{180}Ta the production of ^{180}W increases up to 90%, still in conflict with the comparable predictions from the p-process models.

The s abundances predicted by the classical model at A=180 were further investigated by a parametric study. Variation of temperature and electron density over a wide range of values between T_8=2 to 4 and n_e^{26}=1 to 20, respectively ($n_e^{26} = n_e$ in units of 10^{26} cm^{-3}) shows that a significant fraction of >50% of the solar ^{180m}Ta abundance can be produced provided that the temperature does not exceed T_8=2.8, independent of the electron density. However, such a temperature limit is at odds with the analysis of the Sm-Eu-Gd region, where Arlandini [51] obtained a temperature range of 28<kT<32 keV, in agreement with previous studies [39].

If - regardless of this contradiction - the temperature is assumed low enough to keep the s-contribution to ^{180}W below 30% in order to reproduce the smooth p-process pattern in the mass range around A=180 [6], the electron density would have to be $n_e^{26} > 10$. This result is incompatible with the range $4< n_e^{26} <10$ obtained from the Dy-Ho-Er region [51].

In the stellar model the situation becomes more complex. This is illustrated at the example of the s-process yields obtained in the standard model star of two solar masses ($2M_\odot$) and with half the solar metallicity (Z = 1/2 Z$_\odot$). In the asymptotic giant branch (AGB) phase, stars with 1.5 to 3 M$_\odot$ undergo recurrent He shell flashes. Along with these thermal instabilities, s processing occurs in two steps: between shell flashes with ^{13}C(α,n)^{16}O reactions as the dominant neutron source and during the shell flashes when

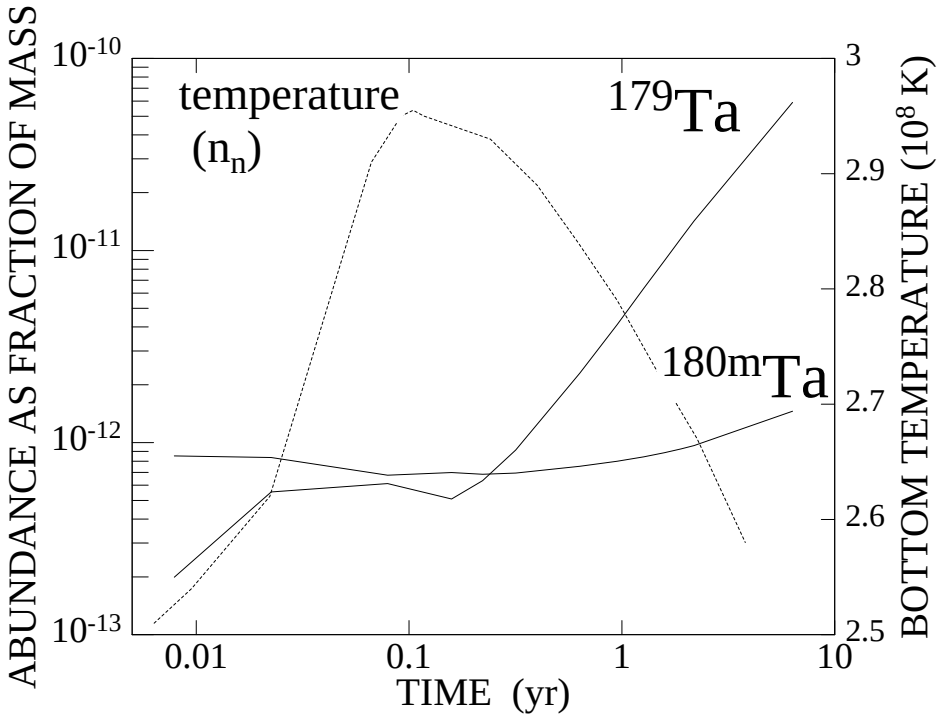

Figure 20: Time evolution of the abundances of ^{179}Ta and ^{180}Ta (plotted as mass fractions) during the ^{22}Ne(α,n)^{25}Mg neutron burst for a typical advanced pulse of the standard model star ($2M_\odot$, $Z = 1/2\ Z_\odot$, see text). The dashed line indicates the bottom temperature of the convective region which reflects also the behaviour of the neutron density.

the temperature is high enough to release neutrons by ^{22}Ne$(\alpha, n)^{25}$Mg reactions.

During the first step the temperature is so low that ^{179}Hf remains stable. Hence the ^{179}Hf branching is closed and ^{180m}Ta is depleted to the level defined by the branching at ^{180m}Hf. The neutron burst from the ^{22}Ne$(\alpha, n)^{25}$Mg source occurs subsequently during a relatively short period ($\Delta t < 10$ y) at the peak temperature reached during the maximum extension of the thermal instability. The enormous energy produced by the 3α reaction at the base of the pulse causes a large gradient in temperature ($0.2 \leq T_8 \leq 3$) and density ($10 \leq \rho \leq 10^4$ g cm^{-3}) in the convective He-burning zone.

This strong gradient implies that - according to the result of the photoactivation measurement [17] - the effective lifetime of ^{180m}Ta varies by more than 15 orders of magnitude between the top and the bottom of the convective zone. Correspondingly, the production and survival of ^{180m}Ta was followed in detail by dividing this convective zone into 25 meshes of equal extension, where the physical conditions could be considered constant per each time-step. The time evolution of each mesh was obtained by the stellar evolution model, which accounts also for the respective changes from pulse to pulse along the AGB evolution [23]. The nucleosynthesis was followed in each mesh separately. The resulting abundances were periodically mixed in intervals of one week, the typical turnover time of the convective zone [24].

It is evident that high temperatures prevail only in a relatively small zone near the bottom of the convective zone, where also the s-process takes place. It is only there that

^{180m}Ta can be efficiently destroyed via thermally induced transitions to the short-lived ground state. However, as long as the turnover time is short compared to the actual half-life, most of the produced ^{180m}Ta is rapidly brought to the outer and cooler zones of the convective region where it survives unaltered. Since this condition is satisfied for the half-life suggested in Ref. [17], thermal coupling of isomer and ground state via the deduced intermediate state at E_x=1.0 MeV has practically no consequence for the s-process production of ^{180m}Ta in the frame of the present stellar model. Though the adopted parameterization of the convective region may be oversimplified, it is commonly used in stellar evolution until a fully hydrodynamical treatment becomes available.

In contrast to the half-life problem, the experimental (n,γ) rate of ^{180m}Ta has a much deeper consequence. Since the s-process yields are to good approximations inversely proportional to the respective Maxwellian-averaged cross sections, the smaller experimental rate implies a corresponding increase of the ^{180m}Ta production compared to the previously adopted calculations, reaching now $\sim$85% of the solar value.

Since ^{180m}Ta is produced during the ^{22}Ne$(\alpha,n)^{25}$Mg burst, its final abundance is practically independent of the exposure due to the ^{13}C$(\alpha,n)^{16}$O source. Analyzing in detail the evolution of the average ^{179}Ta and ^{180m}Ta abundances in the convective shell (Fig. 20), we find a certain delay in the formation of ^{179}Ta as the neutron density rapidly reaches its top. This delay is due to the β^- decay half-life of the 214 keV level in ^{179}Hf. Accordingly, ^{180m}Ta is slightly depleted by neutron captures until the ^{179}Ta abundance builds up. This means that the final abundance of ^{180m}Ta is virtually independent of the uncertain ^{22}Ne$(\alpha,n)^{25}$Mg rate since this affects mainly the peak neutron density.

Finally it is to be noted that stars contributing to the solar distribution exhibit rather similar s-process temperatures. This strongly suggests that ^{180m}Ta can be ascribed almost exclusively to the s process in low mass AGB stars. On the other hand, it is evident that the ^{180m}Ta and ^{180}W abundances can not be reconciled with the phenomenological assumptions of the classical approach, a further severe deficiency of that model in describing the details of the s-process abundance distribution [19].

The main residual uncertainty (apart from the possibility of yet unknown lower-lying intermediate states in ^{180}Ta) is due to the neutron capture cross section of ^{179}Ta. The sensitivity to this parameter was tested by variations of the calculated value recommended by Bao et al. [48]. The corresponding changes of the ^{180m}Ta abundance being about 25% of this variation, a future measurement of this quantity remains a challenge for a satisfactory description of the s-process nucleosynthesis of ^{180m}Ta.

References

[1] H. Palme and H. Beer in Landold-Börnstein, Numerical Data and Functional Relationships in Science and Technology, New Series, Group IV: Astronomy and Astrophysics Vol. 3, p 196, Springer, Berlin Heidelberg New York, 1993.

[2] H. Beer and R.A. Ward, Nature **291**, 308 (1981).

[3] S.E. Kellogg and E.B. Norman, Phys. Rev. C **46**, 1115 (1992).

[4] E. Runte, W.D. Schmidt Ott, W. Eschner, I. Rosner, R. Kirchner, O. Klepper, and K. Rykaczewski, Z. Phys. A **328**, 119 (1987).

[5] K. Yokoi and K. Takahashi, Nature **305**, 198 (1983).

[6] Zs. Németh, F. Käppeler, and G. Reffo, Astrophys. J. **392**, 277 (1992).

[7] C.B. Collins *et al.* , Phys. Rev. C **42**, R1813 (1990).

[8] C.B. Collins, C.D. Eberhard, J.W. Glesener, and J.A. Anderson, Phys. Rev. C **37**, 2267 (1988).

[9] I. Bikit, L. Lakosi, J. Sáfár, and Lj. Čonkić, Phys. Rev. C **59**, 2272 (1999).

[10] S.A. Karamian, C.B. Collins, J.J. Carroll, and J. Adam, Phys. Rev. C **57**, 1812 (1998).

[11] E.B. Norman and S.E. Kellogg, Ap. J. **281**, 360 (1984).

[12] L. Lakosi and T.N. Cong, International Conf. on Nuclear Physics, August, 24-28, 1998, Paris, France, abstract, unpublished.

[13] M. Schumann, F. Käppeler, R. Böttger, and H. Schölermann, Phys. Rev. C **58**, 1790 (1998).

[14] C. Schlegel, P. von Neumann-Cosel, F. Neumeyer, A. Richter, S. Strauch, J. de Boer, C.H. Dasso, and R.J. Peterson, Phys. Rev. C **50**, 2198 (1994).

[15] H. Beer and R.L. Macklin, Phys. Rev. C **26**, 1404 (1982).

[16] J.A. Holmes, S.E. Woosley, W.A. Fowler, and B.A. Zimmerman, Atomic Data and Nucl. Data Tables **18**, 305 (1976).

[17] D. Belic *et al.* , Phys. Rev. Let. **83**, 5242 (1999).

[18] F. Käppeler, R. Gallino, M. Busso, G. Picchio, and C.M. Raiteri, Astrophys. J. **354**, 630 (1990).

[19] C. Arlandini, F. Käppeler, K. Wisshak, R. Gallino, M. Lugaro, M. Busso, and O. Straniero, Astrophys. J. **525**, 886 (1999).

[20] F. Käppeler, K.A. Toukan, M. Schumann, and A. Mengoni, Phys. Rev. C **53**, 1397 (1996).

[21] O. Straniero, R. Gallino, M. Busso, A. Chieffi, C.M. Raiteri, M. Limongi, and M. Salaris, Astrophys. J. **440**, L85 (1995).

[22] O. Straniero, A. Chieffi, M. Limongi, M. Busso, R. Gallino, and C. Arlandini, Astrophys. J. **478**, 332 (1997).

[23] R. Gallino, C. Arlandini, M. Busso, M. Lugaro, C. Travaglio, O. Staniero, A. Chieffi, and M. Limongi, Astrophys. J. **497**, 388 (1998).

[24] D.E. Hollowell and I. Iben, Jr., Astrophys. J. **333**, L25 (1988).

[25] N. Prantzos, M. Hashimoto, M. Rayet, and M. Arnould, Astron. Astrophys. **238**, 455 (1990).

[26] M. Rayet, N. Prantzos, and M. Arnould, Astron. Astrophys. **227**, 271 (1990).

[27] M. Rayet, M. Arnould, M. Hashimoto, N. Prantzos, and K. Nomoto, Astron. Astrophys. **298**, 517 (1995).

[28] S.E. Woosley, D.H. Hartmann, R.D. Hoffman, and W.C. Haxton, Astrophys. J. **356**, 272 (1990).

[29] K. Wisshak, K. Guber, F. Voss, F. Käppeler, and G. Reffo, Phys. Rev. C **48**, 1401 (1993).

[30] K. Wisshak, F. Voss, F. Käppeler, and G. Reffo, Phys. Rev. C **45**, 2470 (1992).

[31] K. Wisshak, K. Guber, F. Käppeler, J. Krisch, H. Müller, G. Rupp, and F. Voss, Nucl. Instr. Meth. A **292**, 595 (1990).

[32] K. Wisshak, F. Voss, F. Käppeler, and G. Reffo, Phys. Rev. C **42**, 1731 (1990).

[33] K. Wisshak, F. Voss, C. Arlandini, F. Käppeler, and L. Kazakov, Phys. Rev. C (in print).

[34] J. Apostolakis, CERN, GEANT library (available from: www.cern.ch).

[35] M. Heil, R. Reifarth, M.M. Fowler, R.C. Haight, F. Käppeler, R.S. Rundberg, E.H. Seabury, J.L. Ullmann, J.B. Wilhelmy, and K. Wisshak, Nucl. Instr. Meth. (submitted).

[36] F. Bečvář, Proc. 10th Int. Symposium on Capture Gamma-Ray Spectroscopy and related Topics, Santa Fe, New Mexico, August 30 - September 3, 1999 (in print).

[37] F. Bečvář, Nucl. Instr. Meth. **A417**, 434 (1998).

[38] K. Wisshak, F. Voss, F. Käppeler, L. Kazakov, and G. Reffo, Report FZKA 5967, Forschungszentrum Karlsruhe, Karlsruhe, Germany 1997.

[39] K. Wisshak, F. Voss, F. Käppeler, K. Guber, L. Kazakov, N. Kornilov, M. Uhl, and G. Reffo, Phys. Rev. C. **52**, 2762 (1995).

[40] F. Voss, K. Wisshak, K. Guber, F.Käppeler, and G. Reffo, Phys. Rev. C **50**, 2582 (1994).

[41] R.L. Macklin, private communication (unpublished).

[42] W. Ratynski and F. Käppeler, Phys. Rev. C **37**, 595 (1988).

[43] T. Rauscher and F.-K. Thielemann, Atomic Data Nucl. Data Tables, **75**, 1 (2000).

[44] J. F. Mughabghab, M. Divadeenam, and N. E. Holden, in *Neutron Cross Sections, Vol. 1, Part A* (Academic Press, New York, 1981).

[45] J.A. Harvey, N.W. Hill, and E.R. Mapoles, Oak Ridge National Laboratory Report No. 5025, 1975.

[46] F. Voss, K. Wisshak, C. Arlandini, F. Käppeler, L. Kazakov, and F. Rauscher, Phys. Rev. C **59**, 1154 (1999).

[47] Z.Y. Bao and F. Käppeler, Atomic Data Nucl. Data Tables **36**, 411 (1987).

[48] Z.Y. Bao, H. Beer, F. Käppeler, F. Voss, K. Wisshak, and T. Rauscher, Atomic Data Nucl. Data Tables, in print.

[49] K. Takahashi and K. Yokoi, Atomic Data Nucl. Data Tables **36**, 375 (1987).

[50] W.M. Howard, B.S. Meyer, and S.E. Woosley, Astrophys. J. **373**, L5 (1991).

[51] C. Arlandini, PhD thesis, University of Heidelberg (2000).